DENSITY FUNCTIONAL THEORY STUDY OF SOLID-STATE STRUCTURE AND OPTOELECTRONIC PROPERTIES OF FLUORENE-BASED CONJUGATED POLYMERS

MOHAMMAD JAVAD ESLAMIBIDGOLI

Density Functional Theory Study of Solid-State Structure and Optoelectronic Properties of Fluorene-Based Conjugated Polymers

by

©Mohammad Javad Eslamibidgoli

A thesis submitted to the School of Graduate Studies in partial fulfillment of the requirements for the degree of Master of Science.

Department of Physics and Physical Oceanography

Memorial University of Newfoundland

August 2012

St. John's Newfoundland

This is dedicated to my loving parents and my brother Mehdi.

Abstract

Using the dispersion corrected density functional theory (DFT-D/B97D) approach, we have performed molecular and solid-state calculations to study the influence of intra- and inter-molecular interactions on the bulk structure and the electronic and optical properties of fluorene-based conjugated polymers. In particular, we investigate the role of side-chain length on the molecular packing and optical properties of poly (9, 9-di-n-alkylfluorene-alt-benzothiadiazole) or FnBT's where n is the number of CH_2 units in the alkyl side-chains. The results indicate that for the FnBT with longer side-chains, due to the significant inter-molecular interactions between the side-chains, the packing of these polymers forms a lamellar structure. On the other hand, for the FnBT with shorter side-chains, the cylindrical phase is more favorable and the corresponding crystals are almost hexagonal. These different packing structures can be attributed to the microphase separations between the flexible side-chains and the rigid backbones and are in agreement with previous investigations for other hairy-rod polymers [1, 2]. In addition, as a result of the efficient inter-chain interactions for the lamellar structures, the dihedral angle between the F and BT units is reduced by about 30° providing a more planar backbone which in turn leads to a decrease, of about 0.2 eV and 0.3 eV, in the band gap of the lamellar structure relative to its value for the gas and cylindrical phases respectively. Time-dependent DFT is also used to study the excited states of the monomer of FnBT with various lengths of side chains.

Acknowledgements

First and foremost, I would like to acknowledge and extend my heartfelt gratitude to my supervisor, Dr. J. B. Lagowski, for her greatest advices and knowledge and her honest encouragement and consultations which guided me through my graduate program and my future studies.

I would also like to acknowledge the financial assistance form Sun Microsystems Canada Inc. (in the form of Graduate Fellowship Administrated by Atlantic Computational Excellence Network (ACEnet) at Memorial University of Newfoundland) and ACEnet for the use of the computational resources. I would like to convey my thanks to Mr. Fred Perry and Dr. Michelle Shaw for their computational help.

Table of Contents

Abbreviations

- **1D** One Dimension(al)
- **2D** Two Dimension(al)
- **3D** Three Dimension(al)
- **ACEnet** Atlantic Computational Excellence Network
- **BT** Benzothiadiazole
- **CC** Coupled Cluster
- **CI** Configuration Interaction
- **CO** Crystalline Orbital
- **CPs** Conjugated Polymers
- **CPU** Central Processing Unit
- **DFT** Density Functional Theory
- **DFT-D** Dispersion Corrected Density Functional Theory
- **EA** Electron affinity
- $\mathbf{E}_{gap}$ Energy Band Gap

- **F8** Octyl-Fluorene
- **F8BT** Poly (9, 9-di-n-octylfluorene-alt-benzothiadiazole)
- **FnBT** Poly (9, 9-di-n-alkylfluorene-alt-benzothiadiazole), where n in FnBT is the number of CH_2 units in alkyl side-chains.
- **GEA** Generalized Expansion Approximation
- **GGA** Generalized Gradient Approximation
- **GTO** Gaussian Type Orbital
- **HF** Hartree-Fock
- **HOCO** Highest Occupied Crystal Orbital
- **HOMO** Highest Occupied Molecular Orbital
- **IP** Ionization Potential
- **LDA** Local Density Approximation
- **LSDA** Local Spin Density Approximation
- **LUCO** Lowest Unoccupied Crystal Orbital
- **LUMO** Lowest Unoccupied Molecular Orbital
- **MP** Møller-Plesset
- **MP2** Mϕller-Plesset Second-order Perturbation Theory
- **NLREG** Nonlinear Regression Analysis Program
- **nqs** no-quota scratch

- **OxF**$_n$ Alternating Fluorene Oxadiazole Copolymers (n=1, 2)
- **PBC** Periodic Boundary Condition
- **PES** Potential Energy Surface
- **PF** Polyfluorene
- **PF2/6** Poly(9, 9-bis(2-ethylhexyl)-fluorene-2,7-diyl)
- **PFH** Poly(9,9-di-n-hexyl-2,7-fluorene)
- **PFO** Poly(9, 9-dioctylfluorene)
- **PW** Plane Waves
- **RAM** Random Access Memory
- **RMS** Root Mean Square
- **SCF** Self Consistent Field
- **TD-DFT** Time Dependent Density Functional Theory
- **UV-Vis** Ultraviolet-Visible

List of Tables

List of Figures

Chapter 1

Introduction

1.1 Conjugated Polymers

Since 1990, when the first demonstration of electroluminescence in conjugated (also referred to as conducting) polymers (CPs) [3] was made, extensive theoretical and experimental investigations have been carried out on the variety of the structures of these materials. CPs are π–conjugated organic materials exhibiting high electronic conductivity when doped and show other optoelectronic properties such as electrochromism [4], electroluminescence [5] and large non-linear optical responses [6]. Many applications have been proposed for this class of polymers and some have been commercially implemented in devices such as organic light emitting diodes [7], photovoltaic cells [8] and field effect transistors [9, 10]. Improved performance of these devices/materials is continually being sought. This effort requires better knowledge of their optoelectronic properties such as band gaps, band widths and energy levels and of their transport properties such as charge mobility and energy transfer. In turn, the investigations of optoelectronic and transport properties require the detailed knowledge of CPs bulk, three-dimensional (3D) structures. For example, when the gas-phase

oligomer approach is used to predict optical band gaps in bulk polymers (with infinite chain lengths), solid-state values are too small by 0.2-0.3 eV due to the neglect of the inter-molecular interactions [11]. For charge transport, the inter-molecular distances and molecular orientations are key factors in determining the charge transfer rates [12, 13, 14].

From the structural point of view, CPs can be categorized as hairy-rod polymers [1, 15] consisting of rigid back-bones and flexible side-chains. Depending on the preparation factors such as temperature and solvent, these materials can self-organize and form a crystalline phases as well as the nematic and isotropic phases [1, 16]. Typically, the studied CPs bulk structures are in the form of films that are spun out of solutions. In the dissolving process, side-chains increase the solubility of polymers by enhancing their attractive interactions with solvent molecules. The resultant CPs bulk structure is essentially controlled by strong intra-molecular interactions along the main chain and weaker inter-chain interactions along the side-by-side and π-stacking [17, 18] directions [1, 16]. In this context, in addition to their solubility effect, the length and the morphology of side-chains can directly affect the molecular packing (aggregate formations) and consequently the bulk structures of CPs [1, 16].

The theory of microphase separation in polymer materials [1, 2, 19] predicts that hairy rod polymers with longer side-chains can form a lamellar structure consisting of two alternating, microphase separated, domains made of the rigid back-bones and the flexible side-chains respectively. On the other hand, polymers with shorter side-chains form crystal structures that can have, for example, hexagonal symmetry and exhibiting side-chain interdigitation. Therefore, it follows that the bulk structure and consequently the optical and electronic and transport properties of CPs are highly

depend on the length of their side-chains [1, 2]. This fact, that the length of side-chains can affect the solubility, solid-state packing, phase behavior and, hence, optoelectronic properties and charge transport of the hairy rod polymers, has been well documented and confirmed by numerous experiments [16, 20, 21, 22].

Polyfluorenes (PFs), one of the most important classes of CPs [23], can be thought of as hairy rod polymers. They are known for having excellent quantum efficiencies, good carrier mobilities and exceptional thermal and chemical stabilities [6]. Among the fluorene derivatives, poly(9,9-dioctylfluorene) (PFO), which is characterized in Figure 1.1, has received extra attention. It exhibits two main morphological formations, referred to as alpha and beta phases, which can modify its photo-physical behavior. They are the amorphous glassy phase (alpha phase), in which PFO molecules have large torsional angles between the adjacent monomers, and the so called beta phase with a high degree of organization and planar PFO molecules. Particular emphasis has focused on the so-called beta-phase, which shows enhanced luminescence, a characteristic well-defined narrow absorption band at 438 nm, and an unusually well-resolved fluorescence. This phase potentially has major technological applications, including blue-light-emitting diodes, optical switches, thin film transistors, solar cells and lasers. However, in bulk phases such as thin films, the alpha-phase and beta-phase normally coexist.

The formation of PFO aggregates is due to both the attractive dispersive π/π interactions between the back-bones and the type of side-chains employed in the polymers. For example, despite the similar chemical structure of the back-bones of PFO and poly(9,9-bis(2-ethylhexyl)-fluorene-2,7-diyl) (PF2/6) (Figure 1.1), each exhibits distinctive phase behavior and optical properties in the bulk form [23]. The major

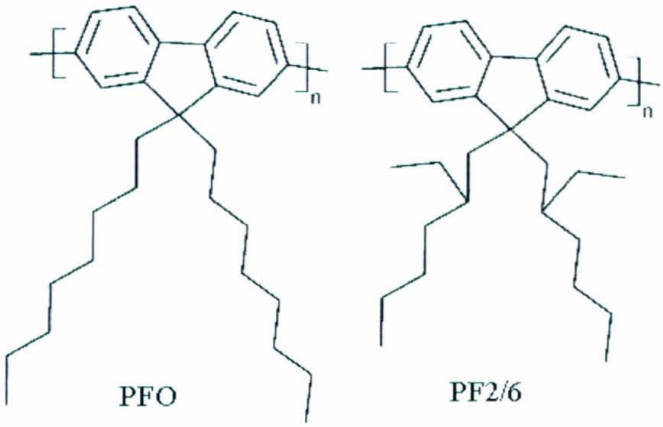

Figure 1.1: Chemical structure of PFO and PF2/6.

difference between these polymers is in their side-chain morphology; while PFO has linear side-chains, PF2/6 has branched side-chains.

In addition to the physical modifications on the side-chains, chemical alterations to the main chains of PFs also provide important mechanism for fine tuning electronic and optical properties for these materials [24]. In a Figure 1.2, number of the alternating copolymers of PF are shown which emit the fluorescence colors in the full visible spectrum.

Poly (9, 9-di-n-octylfluorene-alt-benzothiadiazole) or F8BT, shown in Figure 1.3, is a PF derivative with alternating octylfluorene (F8) and benzothiadiazole (BT) units. F8BT is considered to be a good electron-transporting polymer material [25, 26, 27, 28]. Due to this property, blends of F8BT with hole-transport CPs have been used extensively in organic light emitting diodes and organic photovoltaic cells to balance their carrier mobility and consequently to improve their efficiencies [29, 30].

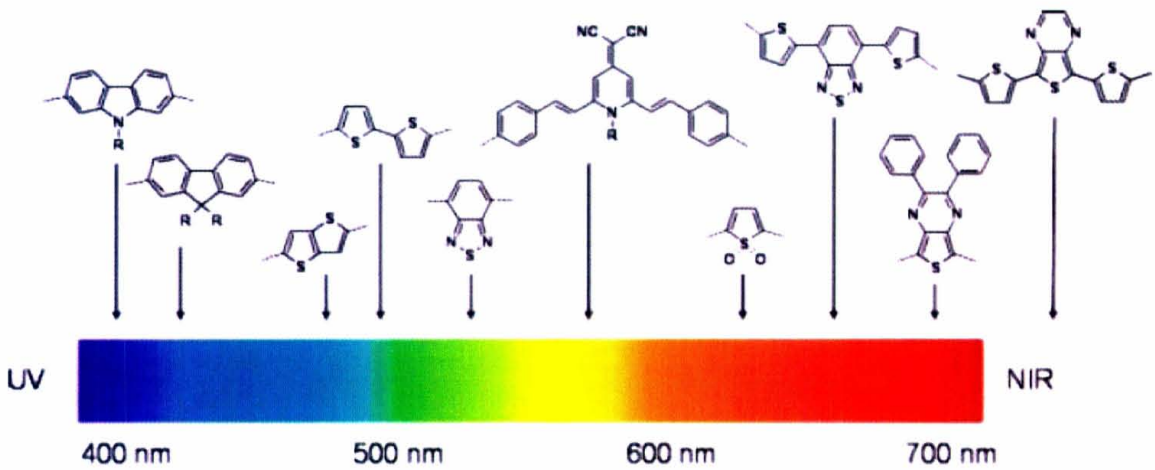

Figure 1.2: Position of the fluorescence colors of several PF co-alternations in the visible spectrum [24].

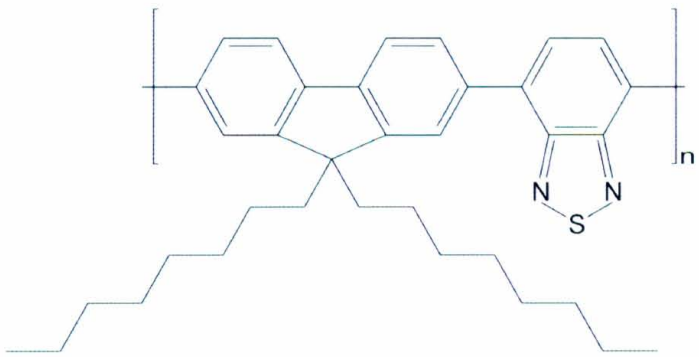

Figure 1.3: Chemical Structure of F8BT.

Many general (system non-specific) computer simulations to model charge transport in CPs have been carried out (see, for example, references [31, 32, 33]). The theoretical/computational approach applied to conjugated polymers is a promising aid in the synthesis of materials with the highest efficiency. These investigations involve many methods, from the empirical mean field simulations to ab initio methods. Numerous quantum mechanical investigations of optoelectronic properties for PFs and derivatives, primarily based on accurate methods such as density functional theory (DFT), were performed on isolated oligomers and polymers in an idealized settings. However, most experiments are performed in solid state and/or in solutions (on specific molecular systems), hence solid-state and solvent effects must be taken into account when computing band gaps and other electronic and transport properties [34].

1.2 Current Research

The main objective of this work is to study the molecular structures of the (infinite) one-dimensional (1D) and 3D crystals of a certain class of fluorene based (e.g. co-alternating fluorene and oxadiazole, and/or fluorene and benzothiadiazole) polymers and oligomers and then to determine their corresponding optical and electronic properties. We use the dispersion corrected DFT [61, 62, 70, 71] (DFT-D) that, in principle, should take into account the long range intermolecular interactions in these solid state calculations. We focus on obtaining detailed knowledge concerning the mechanisms involved in the intra- and inter-molecular interactions between the back-bones and side-chains in the bulk phases of PFs and their co-alternating derivatives. Next, we discuss how the molecular packing can alter the electronic and optical properties of this class of polymers. The obtained results can be of great interest to

experimentalists (e.g. for construction of electronic devices) and others.

The outline of this thesis is as follows: Chapter 2 presents the basic concepts of Hartree-Fock (HF) and DFT methods and the theoretical treatments for periodic systems by using these methods. In Chapter 2 we also give an overview of the basic concepts behind time-dependent DFT (TD-DFT) method. Chapter 3 presents the computational details of Gaussian09 calculations. The major parameters such as the theory level and DFT functionals used in optimization and single point energy calculation are discussed in Chapter 3.

Chapters 4 and 5 discuss the results of the molecular and the solid state (that involves periodic boundary condition (PBC)) calculations for PF and different PF derivatives. In Chapter 4, first the reason for needing to employ the dispersion corrected DFT method in our 3D solid state studies is discussed. Most of the calculations in Chapter 4 are carried out for PFs. The results from Chapter 4 are then used to direct the research to investigate the role of side-chain length on the crystal structure of F8BT. That is, Chapter 5 describes the effect of side-chain length on the bulk structure and electronic and optical properties of F8BT. Finally, Chapter 6 summarizes the conclusions of this thesis.

Chapter 2

Theoretical Framework

Over the past 40 years, DFT based approaches have been widely used in the quantum mechanical computations in molecular and periodic systems as well as the computations of the potential energy surfaces (PES) in single molecules. This chapter presents the basic concepts underlying DFT methods and a general approach adopted for the ab initio study of the electronic structure of periodic systems. This is followed by the description of TD-DFT method used to study the excited states of molecules.

2.1 The Solution of the Schrödinger Equation

Molecular orbital (MO) theory, is primarily concerned with finding an accurate solution of non-relativistic Shrödinger equation in order to obtain the ground and excited state energies and consequently the electronic properties of atomic and molecular systems [35, 36, 37]. By applying the Born-Oppenheimer approximation in which due to the larger mass of a nucleus compared to an electron, the motion of nuclei is assumed to be fixed, the non-relativistic electronic Schrödinger equation in the time-independent form is given as follows:

$$\hat{\mathcal{H}}\Psi(\mathbf{r_1}, \mathbf{r_2}, ..., \mathbf{r_N}) = E\Psi(\mathbf{r_1}, \mathbf{r_2}, ..., \mathbf{r_N}) \tag{2.1}$$

where $\hat{\mathcal{H}}$ is the Hamiltonian operator, Ψ is the wavefunction and E is the total energy of the system. With the use of the Born-Oppenheimer approximation, the Hamiltonian operator, for a system of N electrons, then consists of a sum of three terms: the kinetic energy, the interaction with the external potential, $\hat{v}_{\text{ext}}$, and the electron-electron interaction:

$$\hat{\mathcal{H}} = -\frac{1}{2}\sum_{i=1}^{N}\nabla_i^2 + \hat{v}_{\text{ext}} + \sum_{i}^{N}\sum_{j>i}^{N}\frac{1}{\mid \mathbf{r_i} - \mathbf{r_j} \mid}. \tag{2.2}$$

The external potential is simply the interaction of the electrons with the atomic nuclei:

$$\hat{v}_{\text{ext}} = -\sum_{i=1}^{N}\sum_{\alpha=1}^{M}\frac{Z_\alpha}{\mid \mathbf{r_i} - \mathbf{R}_\alpha \mid}. \tag{2.3}$$

In the above equations, the constants such as the electron mass, electron charge, Planck's constant and the permittivity of free space are assumed to be 1. Also, $\mathbf{r}_i$ is the coordinate of electron i and the charge on the nucleus at $\mathbf{R}_\alpha$ is Z_α.

The Equation 2.1 is solved for a Ψ subject to the constraint that the Ψ is antisymmetric with respect to the interchange of the coordinates of the electrons. In the Hartree-Fock (HF) theory, Ψ can be approximated by a HF wavefunction which can be written as an antisymmetric permutation of a product of a set of (occupied) single electron

functions, ϕ_i (i goes from 1 to N), each of which depends on the coordinates of an electron and which can be succinctly written as a Slater determinant [38]:

$$\Psi_{\mathrm{HF}} = \frac{1}{\sqrt{N!}}\det\left[\phi_1\phi_2...\phi_N\right] \tag{2.4}$$

where the factor $\frac{1}{\sqrt{N!}}$ ensures the wavefunction is normalized. Note that the spin coordinates are omitted here and throughout this chapter to simplify the notation and to concentrate the discussion on the main features of quantum mechanical computations.

Given the electronic Hamiltonian, $\hat{\mathcal{H}}$, and the electronic wavefunction, Ψ, the average total energy is given as the expectation value of $\hat{\mathcal{H}}$ [39], that is:

$$E[\Psi] = \int \Psi^* \hat{\mathcal{H}} \Psi d\tau = \left\langle \Psi \mid \hat{\mathcal{H}} \mid \Psi \right\rangle \tag{2.5}$$

where $d\tau$ stands for spatial coordinates $dxdydz$ for all electrons. The notation $E[\Psi]$ emphasizes the fact that the energy is a functional of a wavefunction. The lowest energy eigenvalue, E_0, and the corresponding ground state wavefunction, Ψ_0, may be found by searching all possible wavefunctions for the one that minimizes the total energy. Also, the probability density of finding electrons with any particular set of coordinates in the ground state is $|\Psi_0|^2$.

The minimization of the total energy is typically performed using the variational method. For the ground state, the variational theorem states that the energy is higher than that of the ground state unless Ψ corresponds to Ψ_0 [40], that is:

$$E[\Psi] \geq E_0. \tag{2.6}$$

In the HF approximation, the HF energy, E_{HF}, is defined as the expectation value of the non-relativistic Hamiltonian for Ψ_{HF}:

$$E_{\mathrm{HF}} = \sum_{i=1}^{N} \int \phi_i^*(\mathbf{r}) \left(-\frac{1}{2}\nabla_i^2 + \hat{v}_{\mathrm{ext}} \right) \phi_i(\mathbf{r}) d\mathbf{r} \tag{2.7}$$

$$+\frac{1}{2}\sum_{i,j}^{N} \int \frac{\phi_i^*(\mathbf{r})\,\phi_i(\mathbf{r})\,\phi_j^*(\mathbf{r}')\,\phi_j(\mathbf{r}')}{\mid \mathbf{r}-\mathbf{r}' \mid} d\mathbf{r} d\mathbf{r}'$$

$$-\frac{1}{2}\sum_{i,j}^{N} \int \frac{\phi_i^*(\mathbf{r})\,\phi_j(\mathbf{r})\,\phi_i(\mathbf{r}')\,\phi_j^*(\mathbf{r}')}{\mid \mathbf{r}-\mathbf{r}' \mid} d\mathbf{r} d\mathbf{r}'.$$

The second and the third terms are respectively the classical Coulomb energy and the the exchange energy written in terms of the orbitals [40]. It should be noted that the exact wavefunction for the ground and excited states of N-electron system can be written as a linear combination of all possible N-electron Slater determinants formed from a complete set of (spin) orbitals $\{\phi_i\}$. The HF energy expression (in Equation 2.7) neglects the energy contributions that arise from the exact wavefunction beyond the HF approximation. These neglected contributions are collectively referred as correlation energy (since the motion of electrons with opposite spins is not correlated in the HF approximation).

In order to find the HF ground state orbitals, we need to apply the variational theorem

to this energy expression under the constraint that the orbitals are orthonormal. This leads to the HF (or the self-consistent field (SCF)) equations:

$$\left[-\frac{1}{2}\nabla^2 + \hat{v}_{\text{ext}} + \int \frac{\rho\left(\mathbf{r}'\right)}{\mid \mathbf{r} - \mathbf{r}' \mid} d\mathbf{r}'\right] \phi_i(\mathbf{r}) + \int v_X\left(\mathbf{r}, \mathbf{r}'\right) \phi_i\left(\mathbf{r}'\right) d\mathbf{r}' = \epsilon_i \phi_i(\mathbf{r}) \tag{2.8}$$

where the non-local exchange potential, v_X is such that:

$$\int v_X(\mathbf{r}, \mathbf{r}') \phi_i\left(\mathbf{r}'\right) d\mathbf{r}' = -\sum_{j=1}^{N} \int \frac{\phi_j(\mathbf{r}) \phi_j^*\left(\mathbf{r}'\right) \phi_i(\mathbf{r}')}{\mid \mathbf{r} - \mathbf{r}' \mid} d\mathbf{r}'. \tag{2.9}$$

The HF equations describe electrons under the influence of a mean field potential consisting of the classical Coulomb potential and a non-local exchange potential. It neglects the interaction between the electrons with the opposite spins. As stated above the difference between the exact non-relativistic (ground or excited state) energy and the HF energy is often referred as the correlation energy. In addition, the computational cost of this approximation is very high and scales quickly with the number of electrons treated. This mainly due to the fact that the accurate solutions require a good description of wavefunction's spatial variation especially near the nuclei. This means that a large basis set is required for the HF wavefunction which adds to the CPU requirements for practical calculations.

2.2 DFT Method

Beyond HF method (which was first introduced by Hartree in 1928 [41]), many correlated methods have been developed for molecular calculations such as Moller-Plesset

(MP), configuration interaction (CI), coupled cluster (CC) and DFT methods [42]. The DFT is amongst the most widely used and computationally accessible post-HF approach that includes the electron correlation. The main variable in DFT is the electron density ρ=$|\Psi\Psi^*|$ rather than the electronic wavefunction Ψ [43, 44, 45].

2.2.1 The Hohenberg-Kohn Theorems

In 1964 Hohenberg and Kohn postulated two theorems that formed the foundation of DFT [46]. The first theorem proves the existence of a unique ground state energy for an N-electron system, that is, it states that the ground state energy of an N-electron system is a unique functional of the ground state electron density, ρ, moving in the presence of a corresponding external potential $v_{\text{ext}}(\mathbf{r})$,

$$E_{v_{\text{ext}}} = E[\rho] = \int \rho v_{\text{ext}}(\mathbf{r}) d\mathbf{r} + F[\rho], \tag{2.10}$$

where F is the universal functional of ρ which contains kinetic, the classical Coulomb and the exchange and the correlation energies. In other words, the electron density is uniquely determined by the external potential. From this statement it immediately follows that the electron density uniquely determines the Hamiltonian operator and consequently the wavefunction and energy and all other electronic properties of N-electron system.

The second Hohenberg-Kohn theorem uses the variational principle to state that the $E_{v_{\text{ext}}}[\rho]$ is a minimum for the ground state density ρ_0, that is, for any positive definite trial density, ρ_t, such that

$$\int \rho_t(\mathbf{r}) d\mathbf{r} = N \tag{2.11}$$

then

$$E\left[\rho_t\right] \geqslant E_r\left[\rho_0\right] = E_0 \tag{2.12}$$

where E_0 is the electronic ground state energy of the system. In its initial form, this theorem restricted DFT to studies of the ground state (since its introduction in 1964 DFT has been extended to many other applications such as excited state computations, systems with finite temperature etc).

The variational principle can be written as:

$$\frac{\delta \mathrm{E}_{v_{\exp}}[\rho]}{\delta \rho} - \mu = 0 \tag{2.13}$$

where μ is the Lagrange multiplier that accounts for the constraint that the integrated density over all space corresponds to the correct number of electrons and is the electronic chemical potential of the N-electron system. When Equation 2.13 is solved, the ground state energy and density correspond to the minimum of the functional $F_{v_{exp}}[\rho]$.

The above discussion establishes the remarkable fact that the universal functional F[ρ] exists, i.e. it does not depend on the external potential, v_{ext} which represents the

particular system of interest. If the form of $F[\rho]$ were known, in principle it could be inserted into the Equation 2.13 which could be minimized to obtain the exact ground state density and energy.

2.2.2 The Energy Functional

From the Schrödinger equation (Equations 2.1 and 2.2), we can see that the energy functional contains three terms — the kinetic energy, the interaction with the external potential and the electron-electron interaction and so we may write the total energy functional as:

$$E[\rho] = F[\rho] + V_{\text{ext}}[\rho]. \tag{2.14}$$

where we define $F[\rho]$ as follows:

$$F[\rho] = T[\rho] + V_{\text{ee}}[\rho]. \tag{2.15}$$

The interaction with the external potential is given by:

$$V_{\text{ext}}[\rho] = \int \hat{v}_{\text{ext}}\rho(\mathbf{r})d\mathbf{r}. \tag{2.16}$$

The kinetic and electron-electron functionals are unknown. If good approximations to these functionals could be found, direct minimization of the energy would be possible.

Kohn and Sham proposed the following approach to approximating the kinetic and

electron-electron functionals [47]. They introduced a fictitious system of N-non-interacting electrons to be described by a single determinant wavefunction in N "orbitals" ϕ_i's. In this system the kinetic energy and electron density are known exactly from the orbitals:

$$T_s[\rho] = -\frac{1}{2}\sum_{i=1}^{N}\left\langle \phi_i \mid \nabla^2 \mid \phi_i \right\rangle \tag{2.17}$$

and

$$\rho(r) = \sum_{i=1}^{N}\left|\phi_i\right|^2 \tag{2.18}$$

It follows then that the exchange-correlation functional has the form:

$$E_{\mathrm{xc}}[\rho] = F[\rho] - T_s[\rho] - E_{\mathrm{H}}[\rho], \tag{2.19}$$

where $E_{\mathrm{H}}[\rho]$ is the classical Coulomb energy (given by second term in Equation 2.7).

Equation 2.19 is simply the error made in using a non-interacting kinetic energy and in treating the electron-electron interaction classically. Writing the total energy functional explicitly in terms of the density built from non-interacting orbitals and applying the variational theorem, we find that the orbitals which minimize the energy, satisfy the following single particle equation:

$$[-\frac{1}{2}\nabla^2 + \hat{v}_{\rm ext}(\mathbf{r}) + \int \frac{\rho\,(\mathbf{r}')}{\mid \mathbf{r} - \mathbf{r}' \mid} d\mathbf{r}' + v_{\rm xc}(\mathbf{r})]\phi_i(\mathbf{r}) = \epsilon_i \phi_i(\mathbf{r}) \tag{2.20}$$

in which we have introduced the local multiplicative potential which is the functional derivative of the exchange-correlation functional with respect to the density:

$$v_{\rm xc}(\mathbf{r}) = \frac{\delta \mathrm{E}_{\rm xc}[\rho]}{\delta \rho}. \tag{2.21}$$

This set of nonlinear equations (so-called Kohn-Sham equations) [47] describes the behaviour of N-interacting electrons in an effective local potential. For the exact functional and thus exact local potential, the orbitals yield the exact ground state density via Equation 2.18 and exact ground state energy via the use of Equation 2.19.

These Kohn-Sham equations have the same structure as the HF equations with the non-local exchange potential replaced by the local exchange-correlation potential $v_{\rm xc}$. Note that as stated above E_{xc} contains an element of the kinetic energy and is not the sum of the exchange and correlation energies as they are understood in HF and correlated wavefunction theories.

The Kohn-Sham density functional theory is an empirical methodology in a sense that we do not know (and have no way of systematically approaching) the exact functional (however, the functional is universal – it does not depend on the materials being studied). Since the form of the exchange-correlation energy functional is unknown, various approximations are used for E_{xc} such as local density approximation (LDA) functional [48] (or local spin density approximation (LSDA) functional [50]),

the generalized gradient approximation (GGA), hybrid functional approach [49] and others.

The LDA can be considered to be the zeroth order approximation to the semi-classical expansion of the density matrix in terms of the density and its derivatives. Typical form of a LDA is:

$$E_{\mathrm{xc}}[\rho] = \int \epsilon_{\mathrm{xc}}[\rho]\rho(\mathbf{r})d\mathbf{r} \tag{2.22}$$

where ϵ_{xc} is the exchange correlation energy for a homogeneous electron gas with density ρ [51].

A natural progression beyond the LDA (or LSDA) is to include gradients of the density ρ, which is referred to as the gradient expansion approximation (GEA) in which first order gradient terms in the expansion are included [52] in the E_{xc}:

$$E_{\mathrm{xc}}[\rho] = \int \rho(\mathbf{r})\epsilon_{\mathrm{xc}}[\rho, \nabla\rho]d\mathbf{r}. \tag{2.23}$$

In the hybrid functional approximation, the exchange functional is taken as a linear combination of the exact HF exchange energy and a DFT exchange functional of the density and the density gradients [53], hence E_{xc} can be written as :

$$E^{\mathrm{xc}}_{\mathrm{hybrid}} = c_{\mathrm{HF}}E^{\mathrm{x}}_{\mathrm{HF}} + c_{\mathrm{DFT}}E^{\mathrm{xc}}_{\mathrm{DFT}} \tag{2.24}$$

where the c_{HF} and c_{DFT} are adjustable coefficients.

In this work, we used one of the most popular hybrid functionals, B3LYP[54] (the so called Becke's three parameter hybrid functional[55]). B3LYP functional has the form[54]: $\mathrm{B3}LYP = 0.2 * \mathrm{X}HF + 0.8 * \mathrm{X}S + 0.72 * \mathrm{X}B88 + 0.19 * \mathrm{V}WN + 0.81 * \mathrm{L}YP$ where XHF, XS, XB88 are the HF, Dirac-Slater, Becke88 [56] exchange functionals and VWN, LYP are Vosko, Wilk, Nusair [57] (i.e., VWN functional III not functional V [54]) and Lee, Yang, Parr [58] correlation functionals. In other molecular cases, we used the (nonhybrid) generalized gradient B97 [59] or the empirically dispersion corrected B97D [60] exchange-correlation functionals in the DFT-D computations. The latter (B97D) was developed and recently reviewed by Grimme [70, 71]. In ab initio calculations, DFT-D approach has been proven accurate for the description of non-covalent interactions between organic molecules. These inter-molecular interactions are type of forces acting between atoms and molecules due to the instantaneous dipole-induced dipole forces, also referred to as Van der Waals or dispersion or London forces. The use of the dispersion corrected DFT is appearing increasingly more often in the literature [61, 62]. The total energy for a system at this level of (dispersion corrected) theory is given by

$$E_{total} = E_{DFT} + E_{disp} \tag{2.25}$$

$$E_{disp} = CR^{-6} \tag{2.26}$$

where, in the above case, the dispersion correction is obtained from semiempirical treatment of non-bonded, inter-molecular interactions and directly affects the equilibrium nuclear geometry.

2.3 DFT Approach to the ab initio Quantum Mechanical Study of Periodic Systems

Given the chemical composition and the crystalline structure of a periodic system, the aim of ab initio computational methods is to calculate its chemical and physical properties as accurately as possible at a reasonable cost. Therefore, an efficient computational scheme must be able to manipulate this information economically with regard to CPU time, storage requirements and the number of input/output operations. In addition the algorithms should be simple and general enough to make accumulation and transfer from one program to another easier [63].

In general, MOs are represented as linear combinations of one electron functions:

$$\psi(\mathbf{r}) = \sum_{\mu=1}^{p} c_\mu \phi_\mu(\mathbf{r}). \tag{2.27}$$

With few expectations, the basic ingredients in solid-state applications for the construction of the basis-set functions, ϕ_μ, are plane waves (PW) and/or Gaussian type orbitals (GTO). The basic advantage obtained from the use of PWs and GTOs is related to the fact that they make the computation of integrals in direct and/or reciprocal space relatively easy. In this work, we employ GTOs as basis functions. In Gaussian based molecular computations, the GTOs are constructed as a linear combination of Gaussian primitives (ϑ_μ's) which are products of spherical harmonics $Y_{lm}(\theta, \phi)$ and radial functions $R(r)$'s for which the basic form is $R(r) = r^l exp(-\alpha r^2)$ [63]:

$$\vartheta_{\mu}(\mathbf{r}) = \sum_{j=1}^{p_{\mu}} d_j g_j(\mathbf{r}) \tag{2.28}$$

where

$$g_j(\mathbf{r}) = g(\mathbf{r}; \alpha, l, m) = r^l Y_{\mathrm{lm}}(\theta, \phi) \exp\left(-\alpha_j r^2\right). \tag{2.29}$$

With a suitable choice of d_j's, the contraction coefficients, and α_j's, the exponents, one can prepare basis functions which have the good characteristics.

In solid state applications, a finite number (p) of GTOs are attributed to the various atoms in the reference zero cell. The same GTOs are then associated with all translationally equivalent atoms in the crystal with the translational vector $\mathbf{T}$. In total, we have Np GTOs, where N is the number of k-points and from which we can construct Np Gaussian-type Bloch orbitals:

$$\Phi_{\mu}(\mathbf{r}; \mathbf{k}) = \sum_{T} \vartheta_{\mu}\left(\mathbf{r} - \mathbf{A}_{\mu} - \mathbf{T}\right) \exp(\mathbf{ik} \cdot \mathbf{T}); (\mu = 1, ..., p; \mathbf{k} = 1, ..., N). \tag{2.30}$$

In other words, with the use of Bloch theorem [63], the GTOs are transformed into 'crystalline orbitals' (COs). In the above equation, A_{μ} denotes the coordinate of the nucleus on which ϕ_{μ} is centered.

In solid state physics, the energy bands are formed by splitting the atomic energy levels when the atoms approach one another in a crystal or a polymer [64]. The band

gap (E_{gap}) is then defined as the energy required for one electron to jump from the top of the valence band to the bottom of the conduction band. In addition to the solid state approach, the band gaps can be approximatly estimated as the energy differences between lowest unoccupied molecular orbital (LUMO) and highest occupied molecular orbital (HOMO) eigenvalues in MO or DFT calculations. In this work, we use both definitions, as derived from solid-state and molecular orbital theories, to calculate E_{gap}'s.

2.4 Time Dependent Density Functional Theory

TD-DFT is an extension of DFT. It uses the fact that the time-dependent wavefunction is equivalent to the time-dependent electronic density. The formal foundation of TD-DFT is the Runge-Gross (RG) theorem (1984) [65] – the time-dependent analogue of the Hohenberg-Kohn (HK) theorem (1964) [46].

The approach of Runge and Gross considers a single-component system in the presence of a time-dependent scalar field for which the Hamiltonian takes the form:

$$\hat{\mathcal{H}}(t)\Big|\,\Psi(t)\Big\rangle = i\frac{\partial}{\partial t}\Big|\,\Psi(t)\Big\rangle\,. \tag{2.31}$$

Again, the Hamiltonian consists of three terms: the kinetic energy operator, the electron-electron interaction and the external potential which along with the number of electrons defines the system. In a similar way, the external potential contains the electrons' interactions with the nuclei of the system. In addition, for non-trivial time-dependence, an additional explicitly time-dependent potential can arise, for exam-

ple, from a time-dependent electric or magnetic field. The many-body wavefunction evolves according to the time-dependent Schrödinger equation under a single initial condition,

$$|\Psi(0)\rangle = |\Psi\rangle. \tag{2.32}$$

Employing the Schrödinger equation as its starting point, the Runge-Gross theorem shows that at any time, the density is uniquely determined by the external potential. This is done in two steps: assuming that the external potential can be expanded in a Taylor series about a given time, it is shown that two external potentials differing by more than an additive constant generate different current densities. Employing the continuity equation, it is then shown that for finite systems, different current densities correspond to different electron densities [65].

The most popular application of TD-DFT is in the calculation of the excited states energies of isolated oligomers [66, 67, 68]. Such calculations are based on the fact that the linear response function, that determines how the electron density changes when the external potential changes, has poles at the exact excitation energies of a system [69].

Chapter 3

Computational Details

All electronic structure calculations were performed with Gaussian09 [54] package available on the computer cluster (Placentia) at the Atlantic Computational Excellence Network (ACEnet) facilities. The DFT-PBC calculations in 3D, with unit-cells with multi-atom basis, are very CPU (Central Processing Unit) and RAM (Random Access Memory) intensive. For example, typically for geometry optimizations, it takes about a month for these calculations to be completed on 4 CPUs. This means that the parallel processing capability of ACEnet is essential to significantly decrease the time required for the completion of each job. The average CPU usage for this project is 4 CPUs per job and the requirement of the memory is 1800-2000 MB for each CPU. We also took the advantage of the no-quota scratch (nqs) space for jobs with large scratch files.

For a number of geometry optimizations of the structures in the oligomer form or in 1D solid state calculations [63], we used one of the most popular hybrid functionals, B3LYP [54]. In other molecular optimization cases, the (nonhybrid) generalized gradient B97 [59] or the empirically dispersion corrected B97D [60] exchange-correlation

functionals were used. The main reason for choosing B97D functional is because of the demonstrated importance of the (non-covalent) dispersion forces [73] in the crystal packing of conducting polymers (see the description of London forces in Chapter 2). Therefore, to optimize the structures in bulk form we used B97D functional [60]. In Chapter 4, we discuss in greater detail the importance of the inclusion of the dispersion forces in the computations by comparing B97D an B97 functionals in a non-bonded fluorene systems.

The basis set used in this work is the polarized split-valence (double zeta) basis set 6-31G(d). It is the expanded version of split-valence 6-31G (which uses one contracted function for 1s and three contracted functions for 2s and 2p orbitals for the first-row atoms, see Chapter 2 Section 2.3 for discussion) that takes into account the polarization effect by including d polarization functions (defined as functions of higher angular momentum than the occupied atomic orbitals) in the basis set [54].

For the solid state calculations [63], we used the PBC keyword [54] in the input file of the Gaussian software. The PBC-DFT method employs GTOs that, with the use of Bloch theorem [63], are transformed into COs. The calculation of energy per unit cell and the optimization of the periodic system use a redundant internal coordinate algorithm which was developed by Kudin et al. [74, 75, 76, 77]. For the PBC calculations the translation vector(s) are required to be appended to the molecule specification, indicating the replication direction(s). Also because of the large size of the molecule in the unit cell, only the Γ point was chosen to sample the first Brillouin zone in 3D solid state calculations. Previous investigation of similar fluorene-based polymers has shown that because of the large molecular basis the electronic band structure of these conjugated polymers is nearly flat [72] and the band gaps at the

Γ ($k = 0$) point and at the Brillouin zone boundary are nearly equal. Therefore, Γ point was deemed sufficient for our 3D solid-state computations. In the 1D solid state (less computationally intensive than 3D) calculations typically larger number of k points were employed. For the purpose of displaying the band structure of 1D PF, we used the keyword IOp(5/103=-1) which allowed us to output the five occupied and unoccupied eigenvalues as a function of k points. In PBC calculations the E_{gap} is obtained as the minimal energy difference between the highest occupied crystal orbital (HOCO) band and the lowest unoccupied crystal orbital (LUCO) band.

In the molecular approach the E_{gap} is determined as the difference between the HOMO and the LUMO eigenvalues. In this thesis, these differences were primarily obtained from the single point energy calculations, mainly discussed in chapter 5 for the structure of poly (9, 9 - di-n-alkylfluorene-alt-benzothiadiazole) or FnBTs (where n is the number of CH_2 units in the alkyl side-chains), performed on the (solid-state) geometries of the monomers with different (n) lengths of side-chains which were optimized with the B97D functional in 3D [60]. Also in Chapter 5, in addition to obtaining bulk structural information of FnBT's, we analyzed their intra-molecular interaction energies (with the use of opt=modredundant keyword) by performing a fully relaxed PES scans. The relaxed PES scan performs a geometry optimization at each step while maintaining the scanned variable constant. On the other hand, the inter-molecular interaction energies were analyzed by carrying out rigid scans for different inter-molecular distances. Rigid PES scans are much easier to perform although they can be less informative in terms of a real dynamic process. In the case of a rigid scan, the scan keyword must be used and the molecular structure must be defined using Z-matrix coordinates (after a blank line, the number of steps and step size for each variable are specified on the variable definition lines, following each variable's

initial value). To find the excited states of our ground state structures, we performed TD-DFT/B3LYP [78, 79, 80, 81, 82] calculations on the monomers of the different optimized structures (corresponding to gas phase, and representative hexagonal and lamellar structures).

In order to obtain the optimized structures we used the keyword opt in the (Gaussian) input files. All molecular and PBC structures were fully geometry optimized to reach the minimum energy state on the PES for the ground state. This condition is satisfied when the first order gradient of energy with respect to the nuclear coordinates is zero. In Table 3.1, the criteria for the SCF convergence are shown. The maximum component of force and the root mean square (RMS) of the force as well as the calculated displacement and the RMS of the displacement for the next step should be below the threshold values [54] as indicated in Table 3.2 for the calculation to be terminated.

Table 3.1: The criteria of the SCF convergence.

Item	Threshold
Maximum Force	0.00045 (N)
RMS	0.0003 (N)
Maximum Displacement	0.0018(Å)
RMS	0.0012(Å)

To generate the input file and to display and measure the quantities of the output geometries we used GaussView 4.1.2 visualization software [84]. The UV-Vis spectra were calculated using the SWizard program, revision 4.6 [83]. The half-bandwidths, were taken to be equal to 3000 cm^{-1}. In order to find the inter-molecular distance in our molecular investigation, we used Nonlinear Regression Analysis Program (NLREG) software which uses the least squared distance approximation to fit a plane

to set of points in 3D. The distance between the two planes were obtained as the inter-molecular distance. Also ACD/ChemSketch (Freeware)12.01 was used to sketch the structures. Wolfram Mathematica 7 was used to plot some data.

Chapter 4

Structure and Electronic Properties of Fluorene Derivatives in Oligomer and Solid-State Systems

In this chapter, first we investigate the accuracy of the semiempirically dispersion corrected DFT method (DFT/B97D) by determining the structure and energy levels of fluorene based conjugated oligomers and polymers. To this end, a comparison has been made between the stable structures and the HOMO and LUMO energy levels of fluorene and fluorene derivatives obtained with this method (DFT/B97D) and those obtained using pure DFT methods with either B97 and B3LYP functionals. Both of these are, in turn, compared with experimental results when available. In addition, by comparing the results of the energy levels, we also illustrate how the intra- and inter-molecular interactions in solid-state structures can influence the values of E_{gap}'s. Finally, we investigate the effect of flexible side-chains in the formation of the bulk

structure of PFs.

4.1 The Importance of Dispersion in Molecular Calculations

In order to investigate the effect of dispersion included in the DFT-D approach, we carried out molecular calculations for a fluorene dimer cluster using both B97 and B97D functionals. We performed rigid potential energy scans as a function of π-stacking distance, d, for two fluorene monomers oriented parallel relative to each other. The results of these scans are plotted in Figure 4.1. One of the curves was determined using DFT/B97 and the other DFT/B97D approach (in both cases the rigid scans are performed on the monomers whose geometries were optimized with B97D functional and later kept fixed when d was varied). The comparison of the two curves in Figure 4.1 clearly shows that the semiempirically corrected dispersion functional, B97D, results in a physical description with a specified stable point whereas B97 does not lead to a minimum.

The MOs for the two optimized (with B97 and B97D functionals) fluorene clusters are shown in Figure 4.2. While the inclusion of dispersion correction affects the equilibrium (nuclear) geometry directly, it also has an indirect effect on the electronic (SCF) DFT calculations since these calculations are carried out on the dispersion corrected (modified) geometries. This observation is confirmed in Figure 4.2 which shows that when B97 functional is used the optimized structure has the planes of fluorene units shifted relative to each other in such a way that they overlap very little. As a result of this reduced overlap, the corresponding MOs of the shifted fluorenes display very little inter-molecular interactions. In turn, when B97D is used,

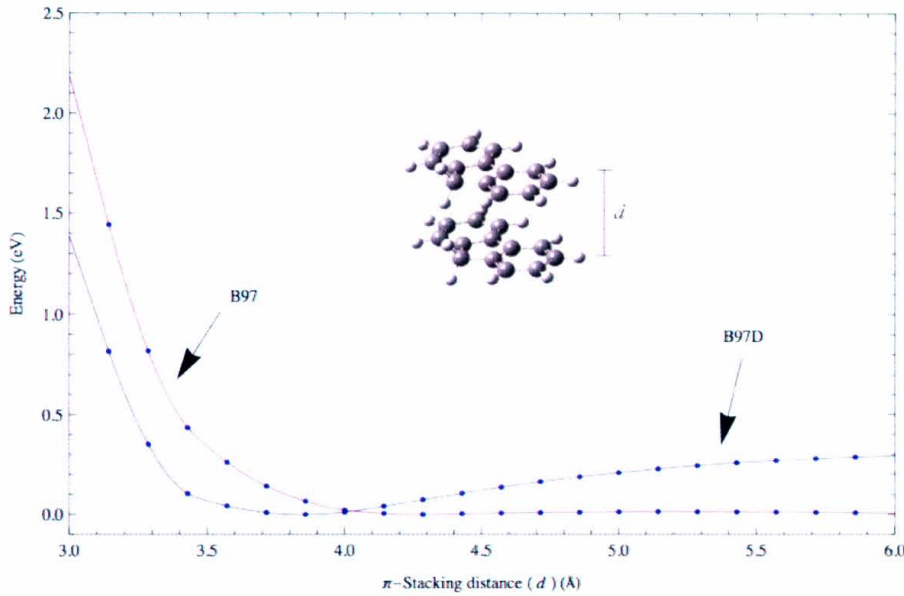

Figure 4.1: Rigid scan of energy versus inter-molecular distance for non-bonded fluorene monomer configuration (the inset of the figure) using DFT/B97 (left) and DFT/B97D (right) functional (geometry of the monomers is fixed at the optimized DFT/B97D values).

the optimized structure has the planes of fluorene units on top of each other and the cluster is more packed in the π stacking configuration. The results of this small study clearly illustrate the importance of using dispersion corrected functionals such as B97D when determining bulk 3D structures.

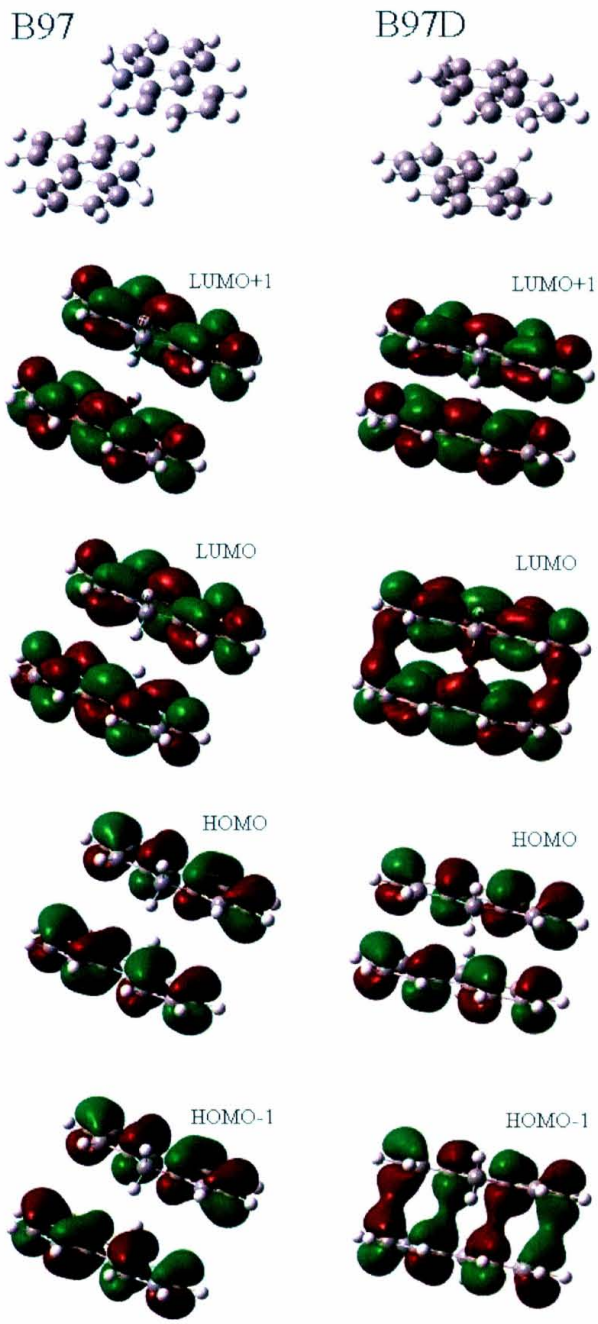

Figure 4.2: Top molecular orbitals obtained for a cluster of two fluorenes that were optimized with DFT/B97 and DFT/B97D functionals as indicated on the figure.

4.2 B97D versus B3LYP in Solid-State Calculations - E_{gap} Determination

B3LYP is one of the most popular functionals to model the electronic structure of organic polymers. In this section, we make a comparison between the obtained geometries and energy levels for the PF structures optimized in 1D solid state calculations with B3LYP and B97D approximations. The goal is to determine the optimal usefulness of these functionals in the solid state studies.

The structure of PF with fluorene dimer in the unit cell (Figure 4.3 (a)) was optimized in 1D using B3LYP and B97D. This structure can be considered as a gas phase structure of PF, since no inter-chain interactions are included. Table 4.1 clearly shows that the best result for the E_{gap} of PF is obtained when the single point energy 1D PBC-DFT/B3LYP calculation is performed on 1D PBC-DFT/B97D optimized geometry (1D instead of 3D was used for simplicity in this case and for better comparison with experiment which uses optical data in dilute solution [86]) which is labeled as B3LYP/B97D. B3LYP/B3LYP gave a similar result as B3LYP/B97D within the one decimal point accuracy when compared to the experimental result. The B97D/B97D and B97D/B3LYP calculations were off by nearly 1 eV.

To test these functionals further, the same calculations have been performed for other fluorene based polymers such alternating fluorene-oxadiazole copolymers or OxFn (n=1,2), whose respective chemical structures are shown in Figure 4.3 (b) and (c). Their results are summarized in Table 4.2 and Table 4.3 respectively. Comparing the results with the experimental values of IP, EA and E_{gap} for PFOx which are in the crystalline phase [87], again considering that in the crystalline phase the band gap

is reduced by 0.2-0.3 eV, we conclude that although the obtained geometries of the structures are pretty similar for the two functionals, the B3LYP/B97D approach gives the energy levels that give best agreement with the experimental results for E_{gap}.

Comparisons between the geometries of the optimized structures (with B97 and B97D functionals) as summarized in the three tables (Tables 4.1-4.3) indicate small differences between the two structures corresponding to the two functionals in each of the three cases. It will be shown in Chapter 5 that this will be the case for FnBTs as well. Therefore, it can be concluded that even though B97D is appropriate for obtaining gas phase and solid state optimized geometries, it seems to underestimate the HOCO energy level of organic conjugated polymers. Therefore, to obtain accurate E_{gap}'s it is more appropriate to use B3LYP functional on the solid state B97D optimized geometries.

Table 4.1: Comparison of various energy parameters (ionization potential (IP), electron affinity (EA), E_{gap}) obtained in single point energy 1D PBC-DFT calculations using DFT functionals as indicated in the first column for PF (without side-chains). The first column indicates the DFT functionals employed in fully optimized 1D PBC-DFT calculations to obtain geometry parameters (of which two, translational vector (TV) and torsional angle (TA) between monomers are included in the table) used in the single point energy computations.

Opt Method	TV(Å)	TA(°)	Single Point Method	IP (eV)	EA (eV)	E_{gap} (eV)
B3LYP	16.9	146	B3LYP	5.02	1.60	3.42
			B97D	4.40	2.08	2.32
B97D	16.9	144	B3LYP	5.02	1.64	3.38
			B97D	4.40	2.11	2.29
Expt. [86, 85]	—	—	—	—	—	3.3

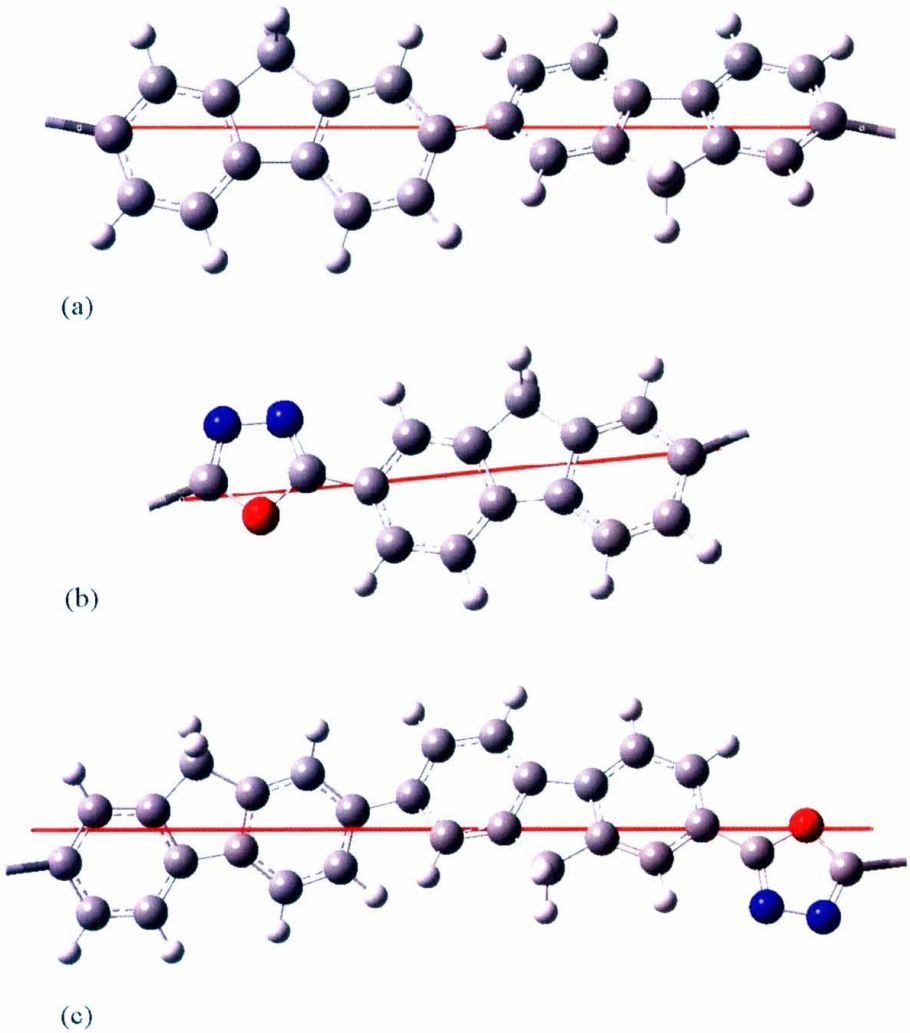

Figure 4.3: Molecular structure of (a) PF, (b) OxF1 and (c) OxF2 unit cells in 1D (without side-chains).

Table 4.2: Comparison of IP, (EA) and E_{gap} obtained in single point energy 1D PBC-DFT calculations using B3LYP and B97D functionals for OxF1 (without side-chains). The first column indicates the DFT functionals employed in fully optimized 1D PBC-DFT calculations to obtain geometry parameters (of which two, translational vector (TV) and torsion angle (TA) are included in the table) used in the single point energy computations.

Opt Method	TV(Å)	TA(°)	Single Point Method	IP (eV)	EA (eV)	E_{gap} (eV)
B3LYP	11.9	180	B3LYP	5.56	2.34	3.22
			B97D	4.91	2.79	2.12
B97D	11.9	180	B3LYP	5.41	2.30	3.11
			B97D	4.89	2.87	2.02
Expt. [87]	—	—	—	6.09	2.93	3.16

4.3 Gas Phase and Cluster Molecular Computations

In this section, we investigate the effect of intra- and inter-molecular interactions on the geometry and energy levels of the optimized fluorene structures (in gas phase and in clusters) by performing molecular DFT/B97D calculations. For the cluster structures, the dependence of the inter-molecular distance on the torsional angle between the fluorene units is also investigated.

4.3.1 Gas Phase Fluorene Monomer and Dimer

The fluorene molecule, characterized in Figure 4.4 (a), is the building block of the structures investigated in this thesis. It contains two benzene rings which are coplanar with the central carbon atom in the molecule [88]. Starting from this structure, the structure of fluorene dimer can be obtained (making sure that it satisfies the inversion point symmetry as required by the long range translational space invariance,

Table 4.3: Comparison of IP, (EA) and E_{gap} obtained in single point energy 1D PBC-DFT calculations using B3LYP and B97D functionals for OxF2 (without side-chains). The first column indicates the DFT functionals employed in fully optimized 1D PBC-DFT calculations to obtain geometry parameters (of which two, translational vector (TV) and torsion angle (TA) are included in the table) used in the single point energy computations.

Opt Method	TV(Å)	TA(°)	Single Point Method	IP (eV)	EA (eV)	E_{gap} (eV)
B3LYP	20.0	134	B3LYP	5.41	1.95	3.46
			B97D	4.75	2.43	2.32
B97D	20.0	133	B3LYP	5.39	2.03	3.36
			B97D	4.74	2.50	2.24
Expt. [87]	—	—	—	5.73	2.79	2.94

see Figure 4.4 (b)). In a similar way, the number of alternating cooligomers and copolymers with different physical properties can be obtained by bonding different molecules to the fluorene molecule (for example see Figure 1.2). For these structures, the intra-molecular interactions along the chain essentially determine the electronic properties of the oligomers and polymers in 1D.

It is known that E_{gap} for a polymer can be extrapolated from finite oligomer calculations since in the limit of infinite number of monomers in the oligomer the polymer limiting value can be reached. As an example of the effect of intra-molecular interactions on the energy levels of the fluorene oligomers, we used B97D to optimize the structures and to find the HOMO, LUMO and E_{gap} of fluorene monomer and dimer. In the Table 4.4 the results are compared with those obtained from 1D PBC-DFT calculations for PF (see Table 4.1) and the experimental value. A comparison between the values indicate that the value of E_{gap} is reduced as the number of monomers is increased. However, this decrease is too much since when the values are extrapolated to the infinite chain length (using the so called oligomer approach), B97D is again

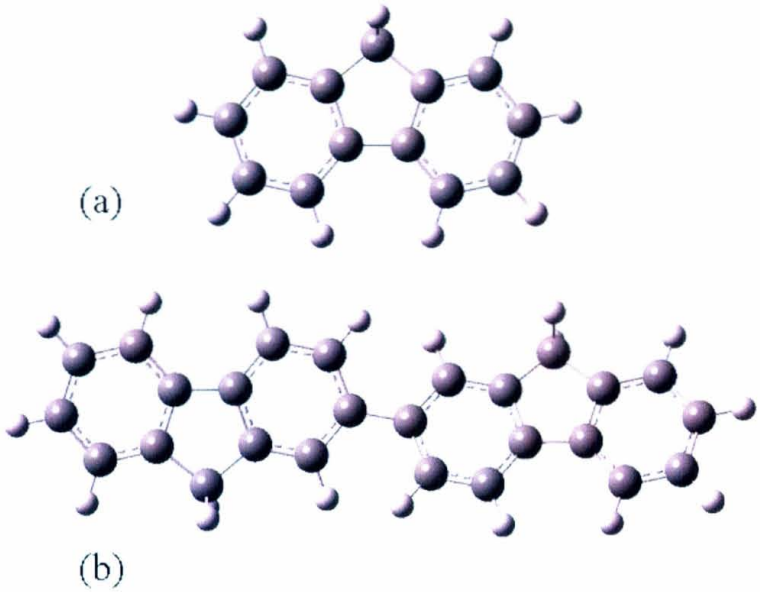

Figure 4.4: Molecular structure of a single (a) fluorene monomer and (b) fluorene dimer.

shown not to be very useful in predicting an accurate E_{gap}.

It should be noted that for the optimized structure of fluorene dimer there is a torsional angle of 146° between the alternating units which as we see in the following sections directly affects the energy levels and therefore the electronic and optical properties of the fluorene based polymers.

Table 4.4: The HOMO, LUMO and E_{gap} of the fluorene monomer, fluorene dimer and 1D PF using B97D/6-31G(d) compared to the experimental values.

Structure	HOMO (eV)	LUMO (eV)	E_{gap} (eV)
Florene	-5.0	-1.3	3.7
Fluorene Dimer	-4.6	-1.8	2.8
Infinite 1D PF	-4.4	-2.1	2.3
Expt.[86, 85]	—	—	3 - 3.4

4.3.2 Non-bonded Fluorene Monomer and Dimer Clusters

To investigate the inter-molecular interactions between the fluorene molecules, the structure of two non-bonded anti-parallel fluorene monomers (2F1) (Figure 4.5 (a)) and two non-bonded anti-parallel fluorene dimers (2F2) (Figure 4.5 (b)) were optimized at B97D/6-31G(d) level. In order to find the inter-molecular distance of the optimized structures, we used the least squared distance approximation to fit a plane to the carbon atoms of each monomer. Then the distance between the two parallel planes was defined as the inter-molecular distance. For this purpose, we used the NL-REG program and the coordinates of the carbon atoms were directly extracted from the gaussian output file. In Figure 4.6, two types of possible parallel planes obtained by this method for the structure of 2F2 are illustrated. Each plane corresponds to a fluorene molecule in a dimer twisted by a torsion angle with respect to the neighbouring fluorene molecule. The inter-molecular distances obtained by this method are 3.4 Å and 3.5 Å for 2F1 and 2F2 respectively. Also due to the molecular packing effect the torsion angle between the fluorene units in 2F2 is decreased by about 5° relative to an isolated dimer F2.

Since in the optimized structure of 2F1 the monomers are shifted relative to each other, in order to estimate the size of this shift, we also found the distance between

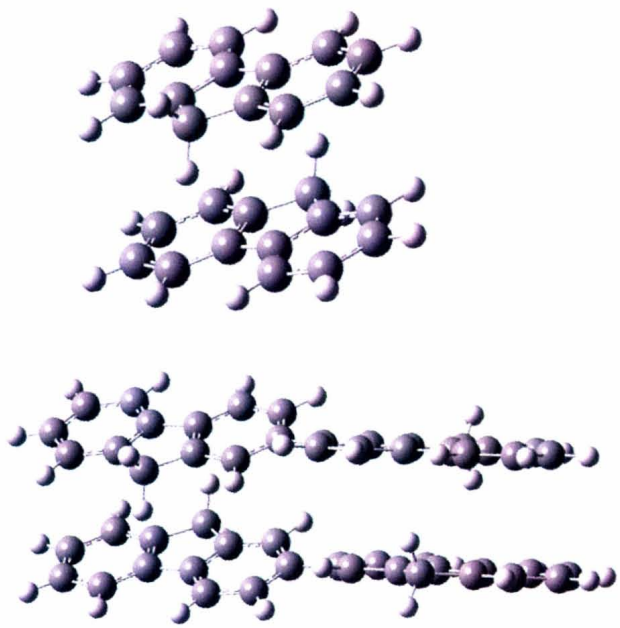

Figure 4.5: Molecular structure of (a) non-bonded fluorene monomer and (b) non-bonded fluorene dimer clusters.

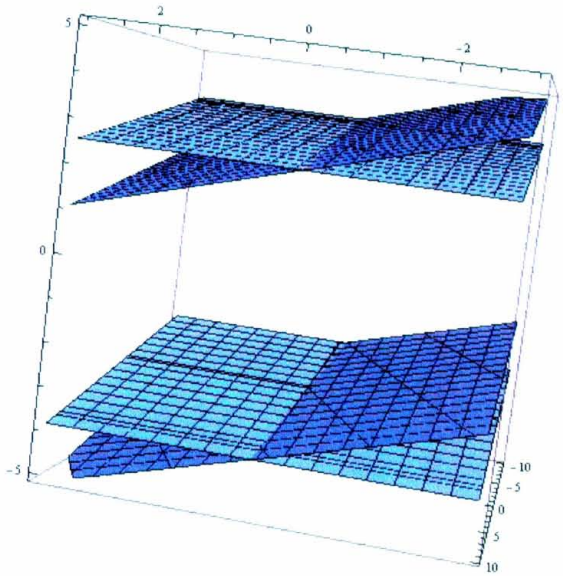

Figure 4.6: Parallel planes corresponding to the structure of non-bonded fluorene dimer cluster obtained by the least squared distance method.

the centers of mass of the two monomers and determined it to be 3.6 Å. By simple trigonometric calculation the amount of translation of the monomers relative to each other is about 1.2 Å. In Table 4.5, the HOMO, LUMO and E_{gap} of these structures are shown. A comparison between the values of E_{gap} for these structures with their corresponding structures in the Table 4.4, which are single (gas phase) fluorene monomer and fluorene dimer respectively clearly shows that the inter-molecular interactions between monomers and dimers decrease the E_{gap}'s value by 0.4 and 0.3 (eV) respectively.

In addition we plotted the energy as a function of the inter-molecular distance, as obtained from rigid scan calculations, for the two structures (Figure 4.7). Comparing the curve in Figure 4.7 (a) with the previous similar calculation using MP2/CP level for 2F1 [90], the stable point is close to 3.5 Å in both cases. However, the depth of

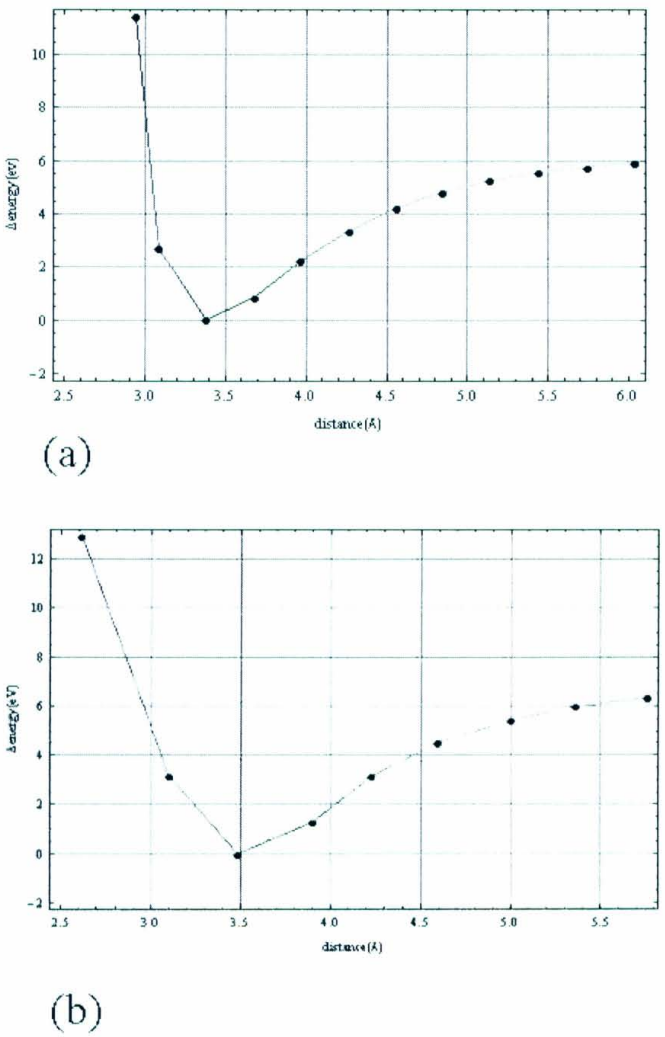

Figure 4.7: Rigid scan of energy versus inter-molecular distance for two (a) non-bonded fluorene monomers and (b) non-bonded fluorene dimers using B97D/6-31G(d).

Table 4.5: The HOMO, LUMO and E_{gap} of the non-bonded fluorene monomer and non-bonded fluorene dimer clusters using B97D/6-31G(d).

Structure	HOMO (eV)	LUMO (eV)	Eg (eV)
Non-bonded Florene Monomers	-4.6	-1.3	3.3
Non-bonded Fluorene Dimers	-4.3	-1.8	2.5
Infinite 1D PF	-4.4	-2.1	2.3

the curve indicating the strength of interaction is very shallow in the MP2/CP level compared to B97D calculation. This agreement for 2F1 between theoretical results obtained using two different ab intio approaches suggests that B97D can be used to accurately describe the interaction between the fluorene molecules. The obtained curve for 2F2 also indicates that B97D/6-31G(d) can give reasonable results for predicting inter-molecular distances for larger systems involving oligomer or polymer clusters.

To see whether or not the inter-molecular distance depends on the torsion angle between the fluorene molecules in 2F2, we performed a constrained optimization with B97D by freezing the torsion angle in a range of 140-180 degrees. However, the distance as indicated in Figure 4.8 (a) is not affected by torsional angle to an accuracy of 0.1 Å. Considering the graph of energy as a function of torsion angle (Figure 4.8 (b)), we conclude that at this level of theory (DFT/B97D) and in the range of 130-180 degrees for torsional angle, 3.5 Å is the most stable inter-molecular distance between the fluorene molecules. This should be compared to experimental value of 4.15 Å for the π stacking distance found in thin PFO films [91].

In summary, B97D/6-31G(d) can be useful to estimate the bulk structure of PF and it gives well defined stable point at a reasonable inter-molecular distance for fluorene clusters. However, this functional is not very useful in estimating the E_{gap} since it

gives rather poor agreement with the corresponding experiment value.

4.4 Solid-State Calculations of PFs

In this section, we used 1D PBC-DFT computations to study the effect of the planarity of the back-bone of PF on the energy levels and the value of E_{gap} of this polymer. The increased planarity is expected as a result of the inter-chain interactions in the bulk form when the chains are close enough. It is also expected that as a result of a more planar back-bone the value of E_{gap} will be decreased. In order to study the bulk effects further, we extend our studies to 2D and 3D systems by including side-chains and again using a DFT solid-state approach.

4.4.1 PF With Planar Back-Bone

It is believed that the inter-molecular interactions in the crystalline phase of PFs may affect the geometry parameters of the back-bone such as the torsional angle between the alternating units [23]. These effects, which are part of so-called bulk effects, may for example decrease the torsional angle between alternating units and result in a more planar back-bone for the polymers which in turn may lead to their different electronic and optical properties. In this section, we investigate the possible effects of the planar back-bone on the electronic properties (E_{gap}) of pure PF in 1D PBC DFT/B3LYP which is characterized by a unit cell as shown in Figure 4.3 (a).

First of all, we need to determine the smallest number of k points (one that does not compromise the accuracy of reciprocal lattice integrations and minimizes the

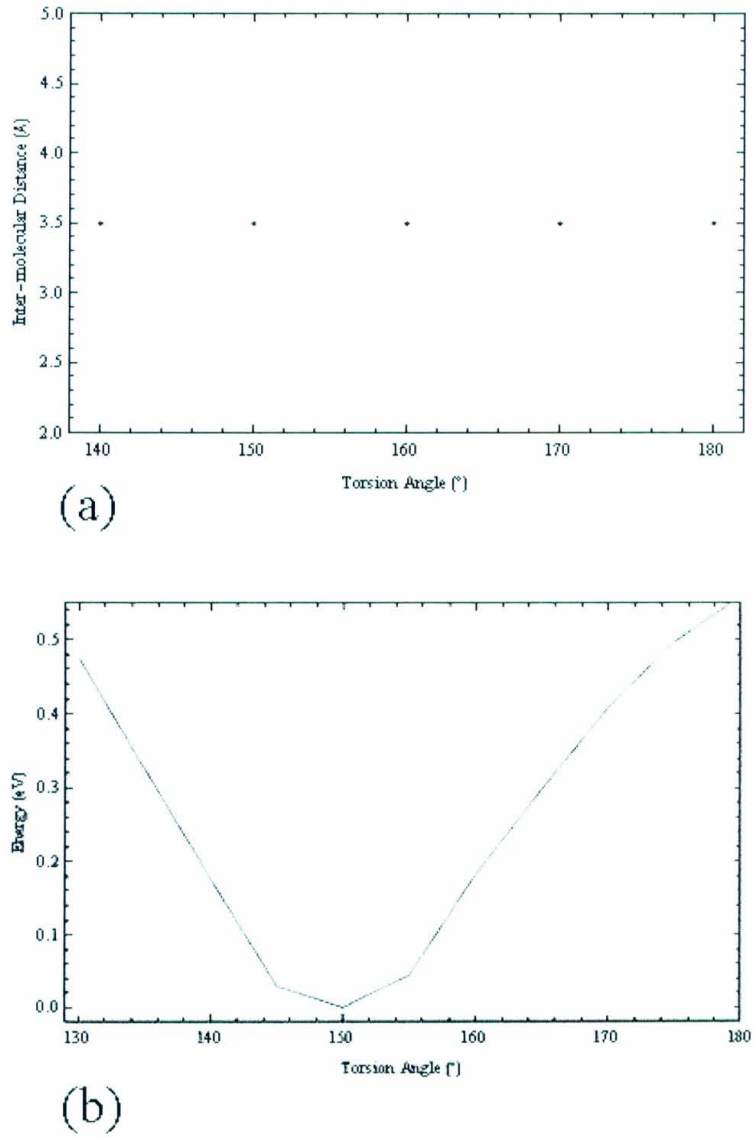

Figure 4.8: (a) Inter-molecular distance versus torsion angle and (b) energy versus torsion angle of the structure of 2F2 using B97D/6-31G(d).

computational costs) to be used in solid state calculations of PFs in 1D. Figure 4.9 show that for PF in 1D, 32-k point calculations are sufficient to model the band structure of these systems since after 32 k points the HOCO, LUCO and the band gap do not change significantly i.e. they converge to their final values.

Next, for the purpose of comparison of PF with planar and non-planar back-bone, the single point energy calculations are performed to find the band structures of pure PF, in the optimized non-planar configuration with a torsion angle of 146 ° between the fluorene molecules, and in the non-optimized planar configuration with zero torsion angle between fluorenes. The results presented in Figure 4.10, still correspond to isolated (gas phase) PF. This figure indicates that the value of the band gap energy for the planar back-bone is decreased by 0.3 eV which is an expected result for these polymers. In the following discussions, we investigate the origin of the bulk effects in more detail.

4.4.2 PF in 1D, 2D and 3D

To find the origin of bulk effects on the structure of PF's back-bone, the first step is to compare the geometry of pure PF in 1D, 2D and 3D. The structure of PF (Figure 4.3 (a)) is optimized in all cases using the PBC DFT/B97D method. In order to minimize the computational costs, side-chains were not added at this step even though they may affect the bulk structure. In Table 4.6, the torsional angles and the inter-chain distances of the optimized structures in 1D, 2D and 3D are listed. Comparing these results to the experimental value of d, which is 4.15 Å (for PFO), the obtained distances in these cases are relatively large (see Table 4.6). Since all three molecular systems give similar structures, their electronic properties are expected to be similar as well.

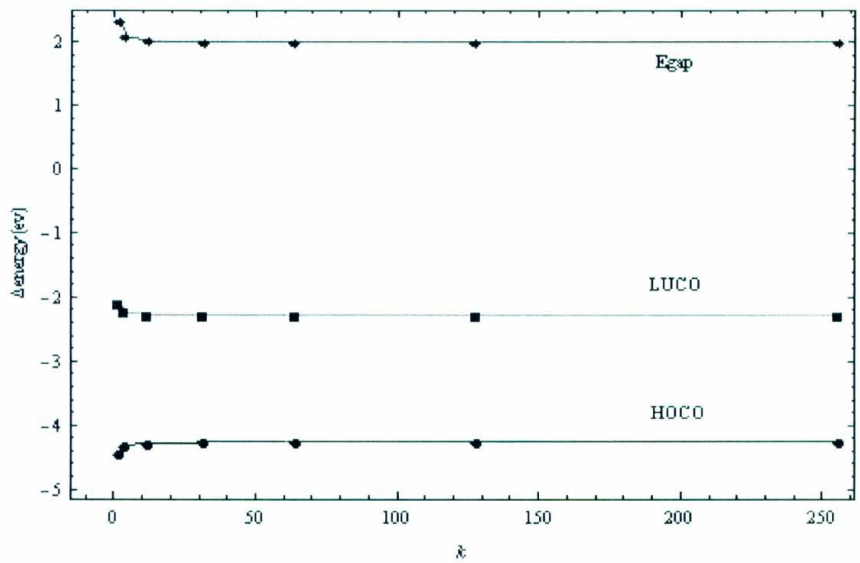

Figure 4.9: HOCO and LUCO energy levels of PF as a function of number of k points at DFT/B3LYP level.

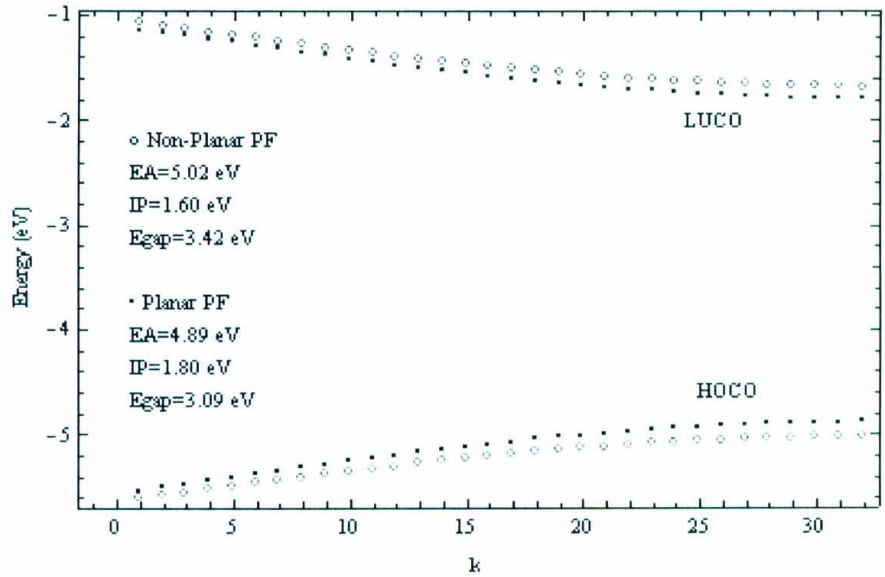

Figure 4.10: DFT/B3LYP 1D band structure of non-planar and planar PF.

Since it appears that bare back-bones (without side-chains) predict relatively large inter-molecular distances for PF even in the 3D solid state calculations, we need to look for other reasons for the bulk effects (as those observed in experiments, e.g. giving d closer to 4.15 Å in bulk PFOs rather than 6.2 Å). We consider the role played by the side-chains in the bulk structure of PFs. In the following parts of the thesis, this role is investigated in more detail for the structure of poly(9,9-di-n-hexyl-2,7-fluorene), or PFH, and F8BT (Chapter 5). PFH was chosen to be studied since its experimental crystal structure is known. Hence comparison between experimental and computational results can be made.

Table 4.6: Comparison of the torsional angles (TA) and the inter-chain distances (d spacing) for the optimized structures of PF in 1D, 2D and 3D using DFT/B97D/6-31G(d).

	TA (°)	d spacing(Å)
1D	144.1	—
2D	146.0	6.23
3D	146.4	6.24

4.4.3 The Crystalline Structure of PFH

Side-chains play an important role in the bulk structure of conducting polymers. Based on their morphologies, their lengths and/or the direction of their organizations, as explained in Chapter 1, different packing structures with the corresponding electronic and optical properties can be obtained for conducting polymers. Also, as it was shown in Section 4.4.2, that without the side-chains the obtained optimized structures in 3D are pretty much the same as the structures in 1D or 2D. In this section,

we report on the result of the solid-state optimization computation for the structure of PF with hexyl side-chains, or PFH, in 3D and compare it with the experimental data [91].

Table 4.7: Crystal parameters [a (along the main chain), b (side-by-side direction) and c (π-stacking direction)] for the structures of PFH.

Crystal Unit Cell	Fluorene Dimer
a(Å)	16.92
b(Å)	14.20
c(Å)	13.14
$\alpha(^\circ)$	124
$\beta(^\circ)$	70
$\gamma(^\circ)$	112
Crystal Symmetry	Nearly Hexagonal

We used 3D PBC-DFT/B97D/6-31G(d) method to optimize the structure of PFH. The directions (a, b, c) and the angles (α, β, γ) relative to the fluorene dimer in the crystal unit cell are defined in Figure 4.11. Table 4.7 summarizes the crystal parameters obtained for the optimized structure. As illustrated in Figure 4.12 (c), PFH forms the nearly hexagonal structure with the side-chains interdigitated between the main chains. This structure is in a reasonably good agreement with the x-ray diffraction study of thin film PFH in which the hexagonal structure is postulated with $|\mathbf{b}|=|\mathbf{c}|=12.4$ Å (with $\alpha = \beta = 90^\circ$ and $\gamma = 120^\circ$) [91]. That is, PFH crystal exhibits hexagonal symmetry and not the lamellar structure which is characterized by π stacking distance close to 4 Å as observed in PFO. It should be noted that since the main chains of PFH crystal are far apart, fluorene units along the back-bone have the additional degree of freedom to rotate relative to each other. Hence the polymer back-bone is not planar and the chain has almost the same geometry as the gas phase polymer. Therefore, we expect the similar electronic properties for this structure as

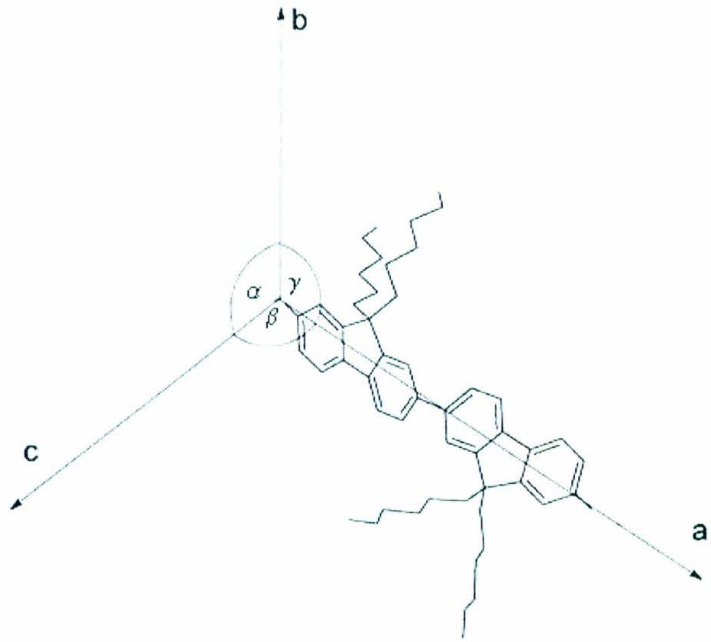

Figure 4.11: Crystal unit cell parameters for PFH.

for the gas phase polymer.

In the next chapter, we investigate the role of side-chain length on the bulk form of F8BT.

4.5 Conclusions

In this chapter we employed DFT-D/B97D, to properly account for properties that depend on inter-molecular interactions such as inter-molecular distance and stable 3D

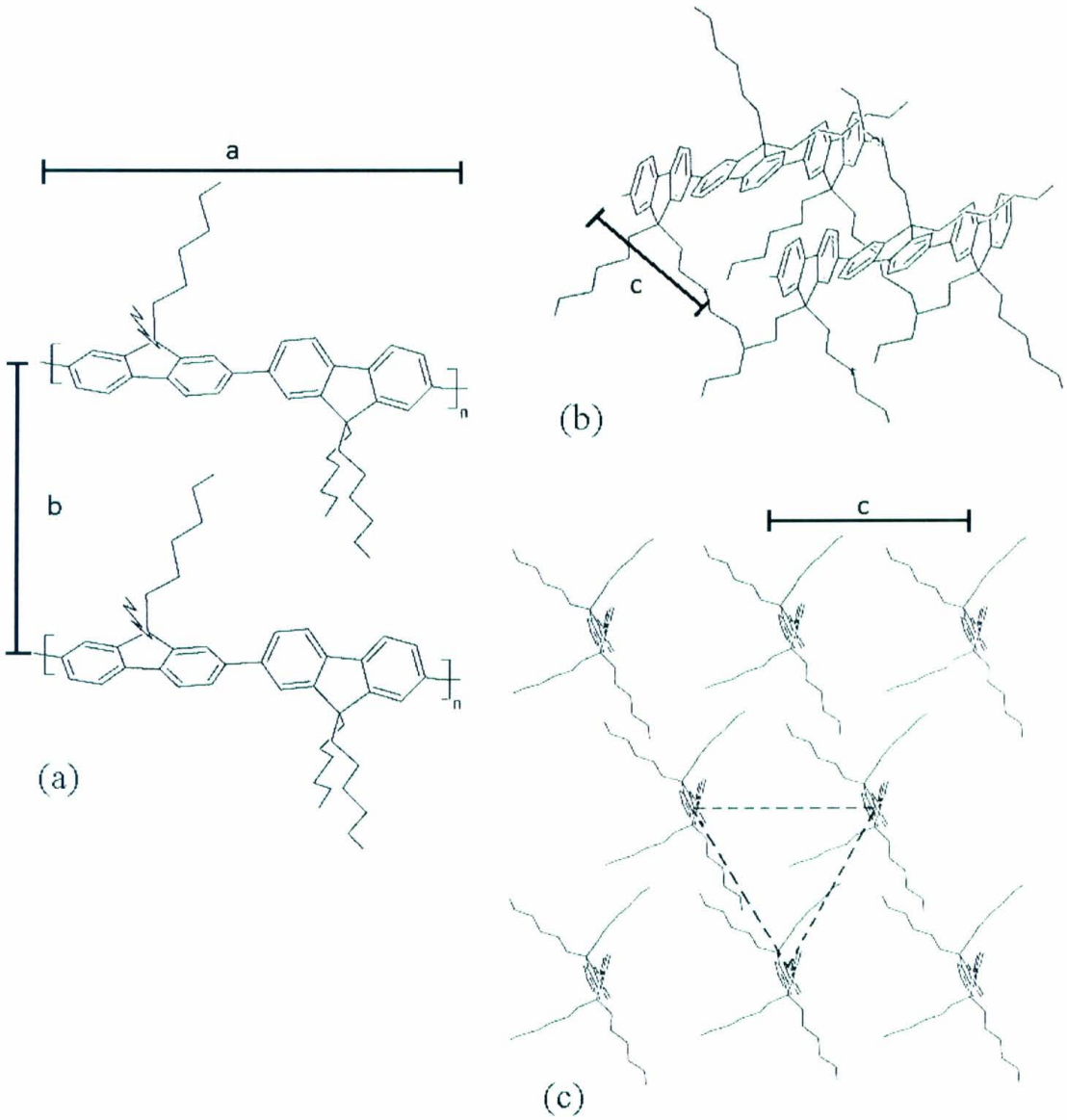

Figure 4.12: Hexagonal structure of PFH, viewed along (a) the side-by-side direction, (b) the π-stacking direction and (c) the π-stacking direction from the top of F6.

bulk structure. It is found that B97D does not give good values for E_{gap}. Therefore, we used B97D to optimize the structures and B3LYP to determine the electronic properties such as E_{gap}'s and the band structures. For the 2D and 3D structures of PF without side-chains, B97D gives the d-distance (corresponding to the π stacking distance) too large (about 6 Å) compared to the experimental value of 4.15 Å for PFO. For the bulk PFH near hexagonal crystal structure was obtained. In the hexagonal structure side-chains keep polymer backbones still far apart, hence backbone planarity in the bulk form is not observed in optimized 3D solid-state computations. In fact, the backbone structure PFH in the bulk is similar to the one observed in 1D gas phase computations.

Chapter 5

The Effect of Side-Chain Length on the Solid-State Structure and Electronic and Optical Properties of Fluorene-alt-Benzothiadiazole Based Conjugated Polymers

In this chapter, by using the dispersion corrected density functional theory (DFT-D/B97D) approach, we have performed bulk solid state calculations to investigate the influence of side-chain length on the molecular packing and the bulk structure of FnBTs (where n is the number of CH_2 units in the alkyl side-chains) (Figure 5.1, also see Figure 1.3). In addition to obtaining bulk structural information of FnBTs, we study how side-chain length affects the inter- and intra-molecular interactions between the back-bone and the side-chains. We also investigate the effect of side-

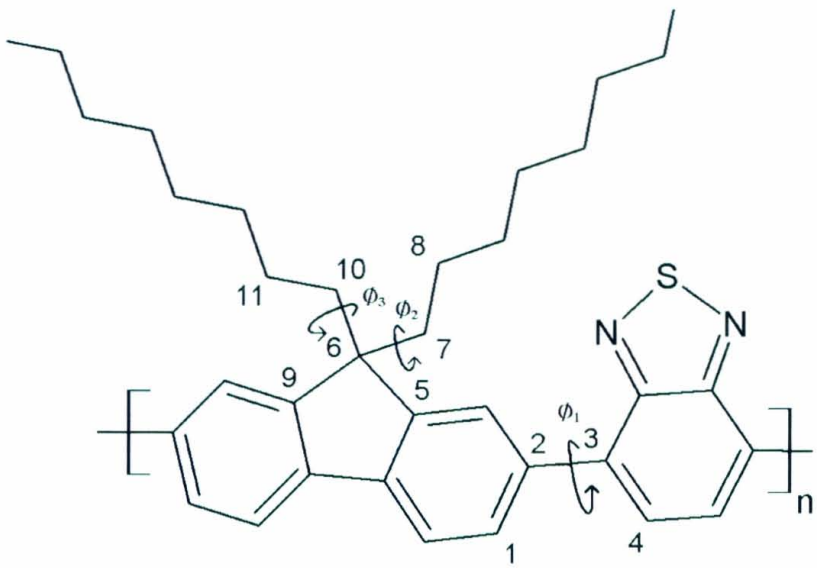

Figure 5.1: Chemical structure of F8BT with the dihedral angles defined as follows: ϕ_1(1,2,3,4), ϕ_2(5,6,7,8), ϕ_3(9,6,10,11).

chain length on the band gaps (E_{gap}) of the FnBTs. Finally, to study the excited states of the monomer of FnBT, molecular non-optimized time-dependent DFT is used on the initially optimized FnBTs in 3D with various lengths of side chains to find the Ultraviolet-Visible (UV-Vis) absorption spectra.

5.1 Influence of the Side-Chains Length on the Packing Structures of FnBTs

In order to investigate the effect of the side chain length (n) on the bulk structure of FnBTs, different flexible alkyl chains from ethyl group (C_2H_5, n=2) to octyl group (C_8H_{17}, n=8) have been attached to the central carbon atom in the fluorene unit and the structures were optimized using 3D PBC-DFT/B97D method. The results,

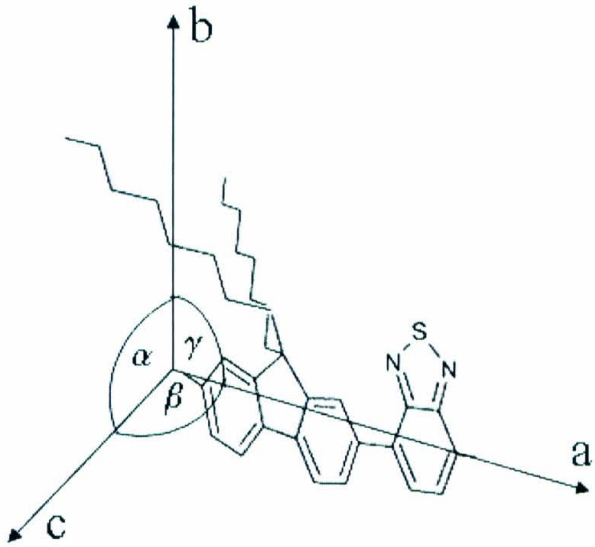

Figure 5.2: Crystal unit cell parameters for FnBT monomers: a (along the main chain), b (side-by-side direction) and c (π-stacking direction) with the corresponding angles.

Table 5.1: Crystal parameters [a (along the main chain), b (side-by-side direction) and c (π-stacking direction)] and the torsional angle (ϕ_1) between the fluorene and BT units for the structures of FnBT with different side-chain lengths (n). Energy band gaps, determined as discussed in the text are also included.

oligomer	FBT	F2BT	F3BT	F4BT	F5BT	F6BT	F7BT	F8BT
a(Å)	12.9	12.9	12.9	12.9	12.9	12.9	12.9	12.9
b(Å)	7.7	10.2	9.5	12.1	13.2	14.3	15.1	15.8
c(Å)	7.1	8.5	10.1	12.1	4.7	4.8	4.7	4.7
$\alpha(^\circ)$	113	119	120	121	84	119	113	103
$\beta(^\circ)$	126	117	112	113	109	109	108	108
$\gamma(^\circ)$	91	89	86	96	118	98	100	103
crystal symmetry	triclinic	nearly	hexagonal		triclinic	/lamellar		
$\phi_1(^\circ)$	40	50	50	50	-16	-17	-16	-14
E_g(B97D) (eV)	2.07	2.12	2.12	2.11	1.91	1.91	1.91	1.91
E_g(B3LYP)(eV)	3.23	3.32	3.32	3.31	3.03	3.04	3.04	3.04
E_g(Ex.[25])(eV)	—	—	—	—	—	—	—	2.9

as summarized in Table 5.1, indicate two different packing structures depending on the side-chain length: the nearly hexagonal and the lamellar structures. Figure 5.2 illustrates how the directions (a, b, and c) and angles (α, β, and γ) are defined relative to the single F8BT monomer (the same definitions are used for all FnBT monomers). In addition, the limiting case of no side-chains (FBT) is also included in Table 5.1. It shows that due to the intra-molecular interactions along the main chain there is a relatively large torsional angle (40°) between the fluorene and BT units which does not allow for efficient π attractions between the main chain planes resulting in the relatively large inter-chain distance (c) and the relatively weak inter-chain interactions. In this case, the chain back-bone has a similar geometry to the optimized structure in 1D PBC-DFT/B97D (single chain), hence essentially reproducing a gas phase result (see also Figure 5.7 in which 1D and 3D band gaps are compared).

By adding side-chains with different lengths, the interplay between the intra- and

inter-molecular interactions of side-chains and main chains can determine which crystal structure is more favorable in the ground state. For the structure with shorter side-chains, consisting of two, three and four carbon atoms, similar to the gas phase, there is a large torsional angle (50°) between the fluorene and BT units. In this case, the side-chains are interdigitated and organize themselves between the main chains along the π-stacking direction causing a relatively large inter-chain distance (c) as indicated for F4BT in Figure 5.3 (note $c = d$ in the Figures 5.3 and 5.4 which show optimized PBC-DFT bulk 3D structures) that increases with the length of the side-chains (see Table 5.1). Figure 5.3 also shows that the chains display alternating structure with BT facing the F unit. The crystal symmetry in this case is almost hexagonal. On the other hand, for the structure with longer side-chains consisting of five to eight carbon atoms, the π-stacking distance is essentially independent of the side-chains length (see Table 5.1) while the distance along the side-by-side direction increases linearly as the length of the side-chains is increased. For these structures, the side-chains arrange themselves along the side-by-side direction, with no alternation of BT and F units, and display a lamellar packing with a considerably smaller π inter-chain distances (see Figure 5.4 and Table 5.1). These smaller π inter-chain distances lead to more efficient inter-chain interactions resulting in a more planar back-bone (see Table 5.1 which shows that for longer side-chains the dihedral angles between F and BT are reduced to approximately 15° from 50° for the shorter side-chains).

In summary, for the FnBTs with longer side-chains, due to the significant intermolecular interactions between the side-chains, the packing of these polymers forms a lamellar structure. On the other hand, for the FnBT with shorter side-chains, the cylindrical phase is more favorable and the corresponding crystals are almost hexagonal. Also, as a result of the efficient inter-chain interactions for the lamellar structures, the dihedral

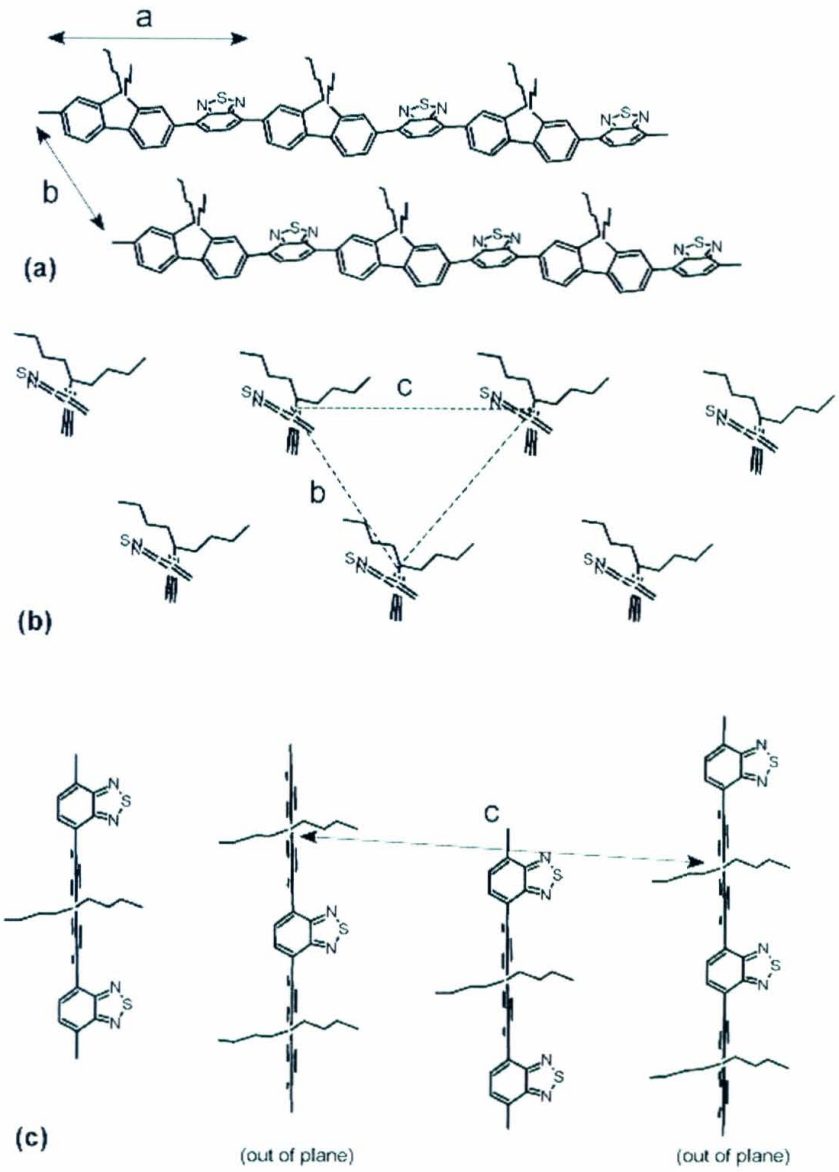

Figure 5.3: The hexagonal structure of F4BT (with shorter side-chains), viewed along (a) the side-by-side direction (chains are not in the same plane), (b) the π-stacking direction from the top, and the π-stacking direction from the side (the in-between chains are out of the plane of the page) of F4 units.

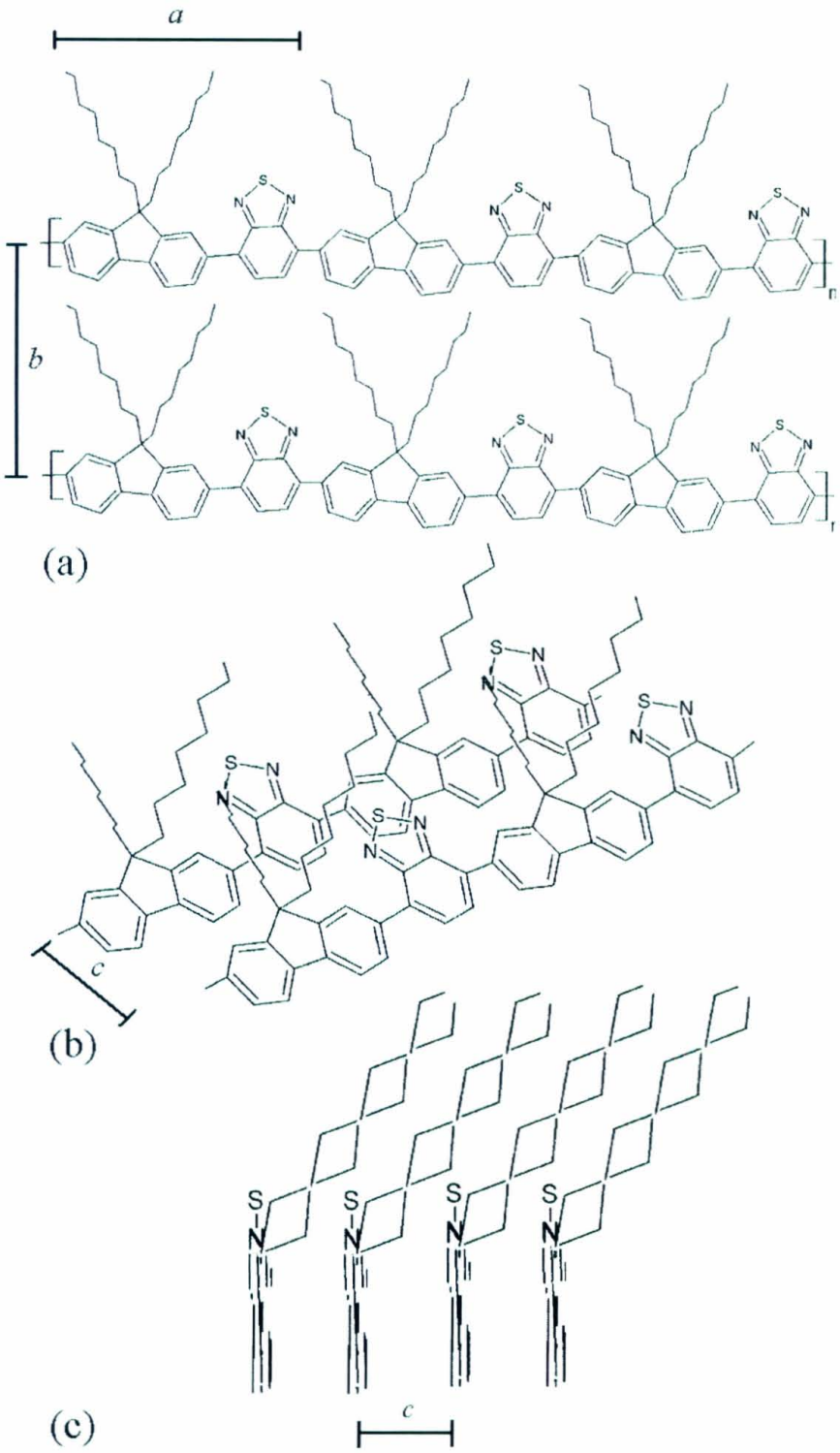

Figure 5.4: The lamellar structure of F8BT (with longer side-chains), viewed along (a) the side-by-side direction, (b) the π-stacking direction and (c) π-stacking direction from the top of F8 units.

angle between the F and BT units is reduced by about 30° providing a more planar configuration for the back-bone. These different packing structures can be attributed to the microphase separations between the flexible side-chains and the rigid back-bones and are in agreement with previous investigations for other hairy-rod polymers [1, 2].

In addition, the inter-molecular interaction energies were analyzed by carrying out rigid potential energy curve scans which employed single point energy 3D PBC-DFT/B97D computations on optimized (also with 3D PBC-DFT/B97D) structures (F2BT and F8BT were chosen as representative examples) as a function of the inter-molecular distance d along the π stacking direction. In these inter-molecular scans, all the other variables (internal inter- and intra-geometry parameters), except d, were kept fixed at the B97D optimized values.

A comparison of the rigid potential energy scans as a function of π-stacking distance (d) for the lamellar structure (as represented by F8BT) with the hexagonal structure (represented by F2BT), as shown in Figure 5.5 (a) and Figure 5.5 (b) respectively, illustrates that the gradient (energy/distance) on the right side of the minimum is considerably steeper for F8BT ($\sim$ 2 eV/Å near the minimum) than for F2BT($\sim$ 0.1 eV/Å). This suggests that the inter-molecular interactions between side-chains and the polymer back-bone for the lamellar structures are much stronger than those for the hexagonal structures. In addition, a direct comparison of the energy curves in Figure 5.5 (a) which correspond to the F8BT with and without side-chains, further supports the conclusion that the longer side-chains are of paramount importance in the formation of the (more) stable bulk structure of FnBTs.

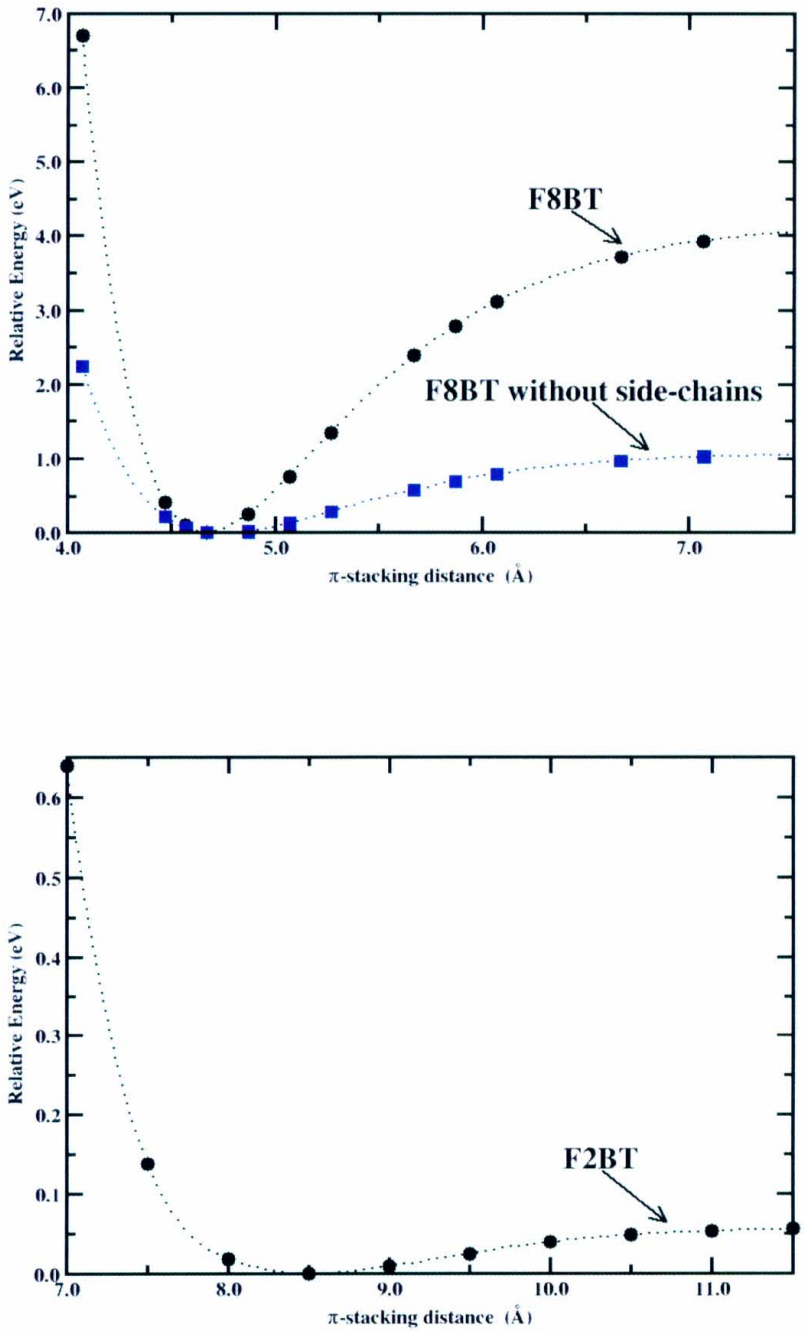

Figure 5.5: The rigid potential energy (eV) determined using 3D PBC-DFT/B97D versus π-stacking distance (d, as shown in Figures 5.3 and 5.4) for the structure of F2BT, F8BT and FBT (F8BT without side-chains).

The effect of side-chain length on the intra-molecular interactions in a single isolated chain was studied by performing fully relaxed potential energy surface scans (with opt=modredundant keyword) on monomers (F2BT and F8BT were also used as representative examples) with their geometries optimized at each scan point using molecular DFT/B3LYP approach. These surface scans involved calculating the relative energies as a function of the two dihedral angles, ϕ_2 and ϕ_3 (see Figure 5.1). To investigate the role of side-chains length in the intra-molecular interactions between side-chains and the back-bone, the relaxed potential energy surface scans as function of two dihedral angles of side-chains, ϕ_2 and ϕ_3 (see Figure 5.1) for the representative monomers of F2BT and F8BT are displayed in Figure 5.6. The energy differences of the corresponding monomers as indicated in the contour plot in Figure 5.6 show a somewhat steeper descent to the minimum for F8BT near the central stable point than for F2BT. This comparison again illustrates that the intra-molecular (as well as inter-molecular) interaction are stronger for polymers with longer side-chains. The comparison between Figures 5.5 and 5.6 (say for F8BT) also shows that inter-molecular interactions between side-chains and polymer back-bones play more dominant role than the corresponding intra-molecular interactions in formation of stable bulk structures.

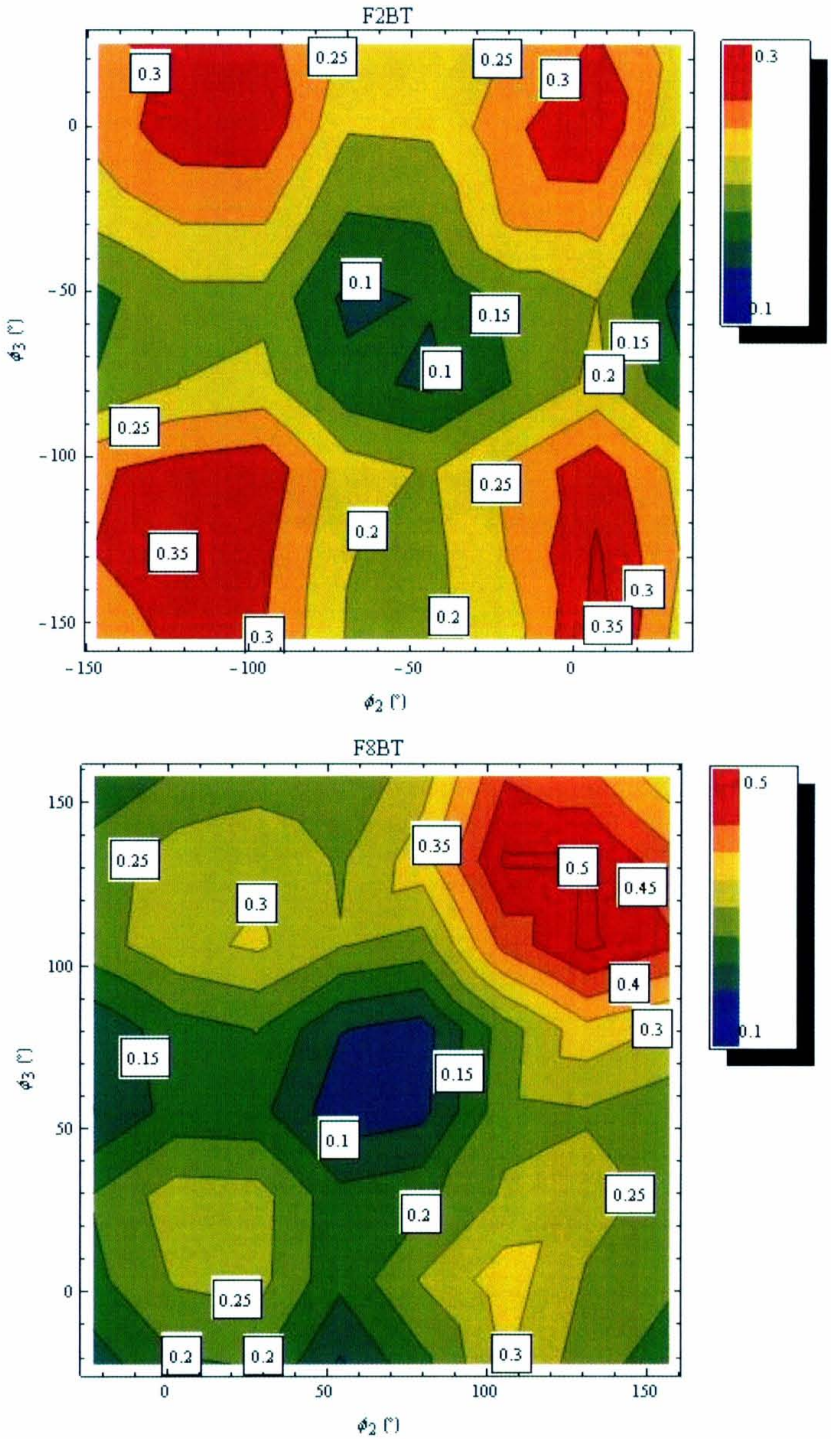

Figure 5.6: The energy contour plots obtained using the fully relaxed potential energy (eV) surface scans (with DFT/B3LYP) versus the dihedral angles ϕ_2 and ϕ_3 as defined in Figure 5.1 for the monomers of F2BT and F8BT.

5.2 Influence of the Side-Chain Length on the Electronic and Optical Properties of FnBTs

In this section, we investigate the effect of side-chain length on the band gaps (E_{gap}) of the FnBTs. In these electronic band gap studies, we carried out molecular single point energy DFT/B3LYP or DFT/B97D calculations on the monomers of FnBTs whose geometry parameters were fixed at the optimized values obtained in the fully relaxed 3D PBC-DFT/B97D computations (referred to as B3LYP/B97D or B97D/B97D for short). In this approach, the band gaps of FnBTs were estimated as the energy differences between the HOMO and LUMO energies as obtained in the molecular DFT calculations. As is shown in Table 5.1, the solid state packing of the structures with longer side-chains (FnBT with n=5-8) leads to a decrease in the torsional angle between fluorene and BT units providing a more planar configuration for the backbone in the lamellar structure. This physical modification in the geometry of the backbones directly affects the energy levels and consequently the electronic and optical properties of the FnBTs. In Figure 5.7, the LUMO-HOMO band gaps (E_{gap}'s) are plotted as a function of side-chains length (n) for the monomers of FnBTs which, in turn, were optimized in their ground states with the use of 1D and 3D solid-state calculations (see Computational Details section for methodology).

For the most part and as expected, the length of the side-chains does not affect the value of the band gap of the FnBT monomers in 1D cases (E_{gap} for 1D FBT is slightly higher (3.21 eV) in comparison to the remaining values, all close to 3.17 eV, for the other monomers with finite n). Also, as indicated earlier, the 3D and 1D band gaps for FBT give nearly the same value and hence we can say that in this case FBT bulk structure is the same as the gas phase. In the 3D cases, due to the solid-state effects,

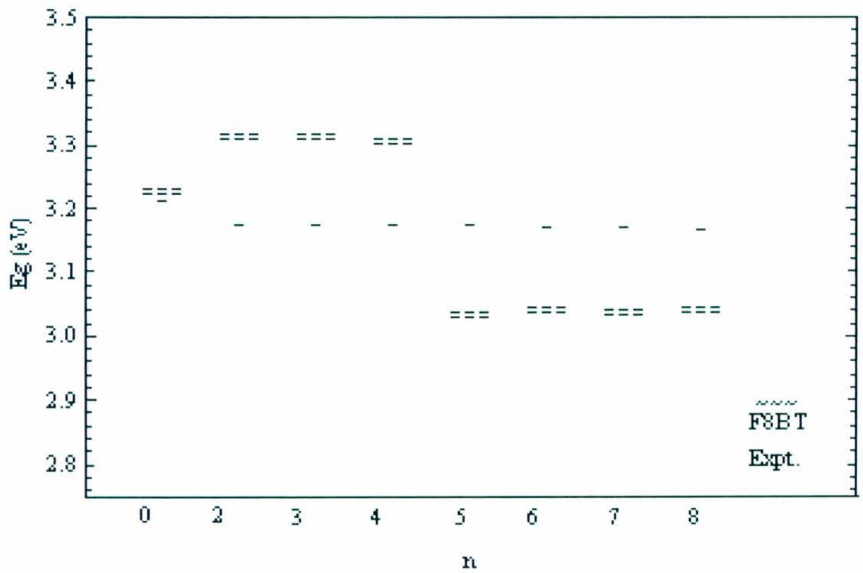

Figure 5.7: The LUMO-HOMO band gaps (E_{gap}'s) calculated with DFT/B3LYP using the optimized (with solid-state 1D (-) or 3D (===) PBC-DFT/B97D) structures of the monomers of FnBT with different number (n) of CH_2 units in side-chains. Experimental value [25] for F8BT is also shown.

the band gap is decreased by 0.2 and 0.3 eV for the lamellar structures corresponding to polymers with longer side-chains relative to the gas phase (1D) and the hexagonal structures with shorter side-chains respectively. It should be noted that the band gap for the nearly hexagonal structures increases by 0.1 eV in comparison to its gas phase value which is unusual since most of the time bulk effects tend to reduce the band gap values. However, in this case, this behavior is not unexpected since, as can be see from Table 5.1, the torsional angle between F and BT actually increases in the hexagonal packing relative to gas phase and it is well known that band gap values increase when planarity along the back-bone is decreased. Also, taking the accuracy of calculated values to 1 decimal point, the value of the band gap energy for the lamellar structure of F8BT is off by 0.1 eV when compared with its experimental result [25]. This indicates that not all the intra- and inter-molecular interactions are accounted for in the 3D PBC-DFT/B97D structural calculations.

Finally to find the excited states of FnBTs, we performed molecular, non-optimized time-dependent DFT, TD-DFT/B3LYP [78, 79, 80, 81, 82] calculations, again, on the monomers in the various solid-state B97D optimized structures (obtained in 1D PBC-DFT/B97D for the gas phase, and 3D PBC-DFT/B97D for representative hexagonal and lamellar structures computations). Using the TD-DFT data, UV-Vis absorption spectra were determined with the help of the SWizard program [83]. Clearly, the molecular packing and conformational changes along the chain back-bones must also effect the absorption spectra in say photoluminescence experiments. Using the TD-DFT approach as described in the Computational Details sections, three representative absorption spectra are obtained and are displayed in Figure 5.8. They correspond to three different packing structures: the gas phase (FBT), hexagonal (F4BT) and lamellar (F8BT). The spectra show two peaks associated with the two

separate electronic transitions in corresponding FnBTs. The spectrum for the lamellar structure is shifted to longer wavelengths relative to the gas phase and the hexagonal phase, not surprising considering the greater planarity of their chain back-bones. A good agreement with the experimental result [89] (which is also included in Figure 5.8) is obtained for the absorption spectrum of crystalline F8BT. Both the computational and experimental data for F8BT display a broader peak that is centered near 465 nm and the narrower one that is centered near 320 nm.

5.3 Conclusions

In conclusion, the dominant London forces (see Chapter 2) between the side-chains in the structures of FnBT with longer side-chains (n>4) can induce a microphase separation between the flexible side-chains and the rigid back-bone, providing an organized phase of side-chains along the side-by-side direction and forming a lamellar phase with a constant and smaller π-stacking distance between the main chains. This molecular packing leads to a more planar geometry of the back-bone which directly alters the electronic and optical properties of the system. For example it reduces the molecular band gap by about 0.2 eV and 0.3 eV in comparison to the gas phase and the cylindrical phase respectively. Also, the absorption spectra for this phase is red shifted in comparison to the other phases. On the other hand, for the cylindrical (hexagonal) phase, the side-chains are too short to efficiently interact. Therefore, for this hexagonal phase side-chains interdigitate and are localized between the main-chains along the π-stacking direction and, hence, cause a larger inter-chain distance and consequently smaller inter-molecular interactions. These different packing structures are in agreement with previous investigations for other hairy-rod polymers [1, 2].

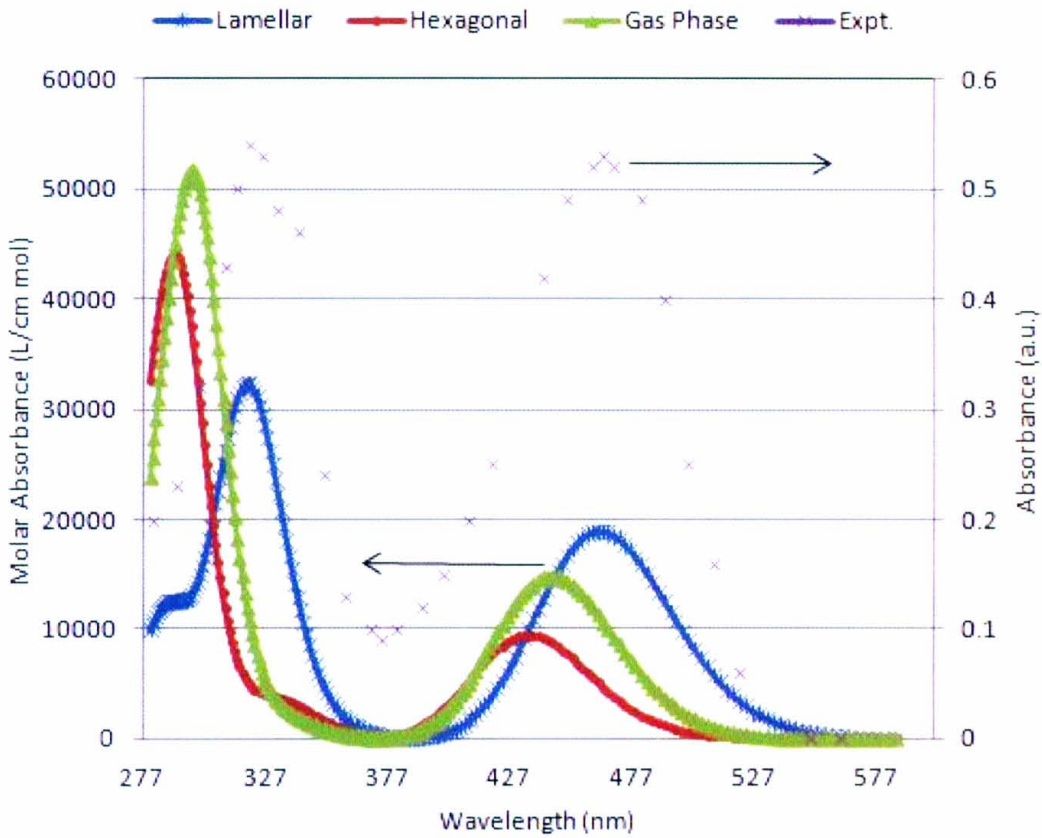

Figure 5.8: Absorption spectra of the various monomers in the representative optimized (with PBC-DFT/B97D) structures of FnBT in 1D (gas phase, n=0) and in 3D (hexagonal (n=4) and lamellar (n=8) structures) using TD-DFT/B3LYP and compared to experimental data for F8BT [89]. Note the experimental data plot uses the right y-axis

Our results for the optical properties of F8BT in lamellar phase are in good agreement with the experimental data. The results obtained in this work also indicate that the dispersion corrected functionals such as B97D are important in determining correct 3D solid-state structures. However, the electronic and optical properties such as band gaps and absorbtion spectra are best described using a hybrid approach that employs the PBC-DFT/B97D geometries in the molecular structure DFT/B3LYP or TD-DFT/B3LYP calculations.

Chapter 6

Summary and Conclusions

In this chapter, we summarize the major results of this work. Our calculations indicate the importance of the dispersion term included in B97D functional for molecular calculations which results in physical structural description of non-bonded fluorene systems. In addition, a comparison between the results of the 1D solid-state fluorene polymers obtained from B97D with those obtained from B3LYP shows that although the geometry parameters of the optimized structures are close, B3LYP single point calculations on PBC DFT/B97D structures leads to more accurate results for estimating the energy levels and the band gaps.

Further the intra- and inter-molecular interactions seem to affect the geometry parameters of the fluorene and fluorene derivatives. For example, when the torsional angle between the fluorene units is reduced in non-bonded cluster of fluorene dimers, the energy levels and electronic properties of the system can change. In polymers (with lamellar bulk structure), the inter-chain interactions results in chains with more planar back-bone and consequently reduced band gaps by about 0.2-0.3 eV. We investigated the origin of these inter-chain interactions by performing 3D PBC DFT calculations

on the structures of PFH and F8BT. In particular, the role of side-chains length on the crystalline structure and inter-chain packing of these structure was studied. For the structure of PFH the nearly hexagonal structure were obtained with a relatively large inter-chain distance that is occupied by side-chains. For the bulk FnBT where n represents number of CH_2 units in the alkyl side-chains (studied systems n=2-8), we found that depending on the length of the side-chains different packing forms were obtained: for up to n=4 a cylindrical phase and from n=5 upwards a lamellar form was found. For the lamellar form a smaller torsional angle between the fluorene and benzothiadiazole is obtained than for the cylindrical phase, resulting in a smaller band gap which is confirmed by excited state TD-DFT calculations.

In conclusion, the detailed knowledge of the bulk structure of conjugated polymers (e.g. packing, crystal symmetry, the orientation of side-chains, etc.) is essential to determine the optical and electronic properties as well as the charge carrier mobility in these materials. This work has the potential to provide new physical insights into the packing effects on structure and electronic properties of conjugated polymers. In particular, the crystal symmetry and inter-molecular packing information of F8BT can be used to further study the charge transport and mobility simulation of this polymer.

Bibliography

[1] R. Stepanyan, A. Subbotin, M. Knaapila, O. Ikkala, G. ten Brinke, *Self-Organization of Hairy-Rod Polymers*, Macromolecules **36** (2003) 3758–3763.

[2] David L. Cheung and Alessandro Troisi, *Molecular Structure and Phase Behaviour of Hairy-Rod Polymers*, Phys. Chem. Chem. Phys. **11** (2009) 2105–2112.

[3] J.H. Burroughes, D. D. C. Bradley, A. R. Brown, R. N. Marks, K. Mackay, R. H. Friend, P. L. Burns, A. B. Holmes, *Light-Emitting Diodes Based on Conjugated Polymers*, Nature **347** (1990) 539–541.

[4] Kenji Hyodo, *Electrochromism of Conducting Polymers*, Electrochimica Acta **39** (1994) 265–276.

[5] J. H. Burroughes, D. D. C. Bradley, A. R. Brown, R. N. Marks, K. Mackay, R. H. Friend, P. L. Burns and A. B. Holmes, *Light-Emitting Diodes Based on Conjugated Polymers*, Nature **347** (1990) 539-541.

[6] T. A. Skotheim and J. R. Reynolds (Eds.), *Conjugated Polymers: Theory, Synthesis Properties, and Characterization (Handbook of Conducting Polymers)*, CRC Press, New York (2006).

[7] Alan J. Heeger, *Semiconducting and Metallic Polymers: The Fourth Generation of Polymeric Materials*, J. Phys. Chem. B **105** (2001) 8475–8491.

[8] S. Sun and N. Sariciftci (Ed.s), *Organic Photovoltaics* CRC Press, Boca Raton, FL (2004).

[9] Ananth Dodabalapur, *Organic and Polymer Transistors for Electronics*, Materials Today, **9** (2006) 24–30.

[10] H. Klauk (Ed.), *Organic Electronics*, Wiley-VCH Verlag, GmbH and Co. KGaA, Weinheim (2006).

[11] Johannes Gierschner, Jerome Cornil, and Hans-Joachim Egelhaaf, *Optical Bandgaps of π-Conjugated Organic Materials at the Polymer Limit: Experiment and Theory*, Adv. Mater. **19** (2007) 173–191.

[12] Nicolas Blouin, Alexandre Michaud, David Gendron, Salem Wakim, Emily Blair, Rodica Neagu-Plesu, Michel Belletete, Gilles Durocher, Ye Tao, and Mario Leclerc, *Toward A Rational Design of Poly(2,7-Carbazole) Derivatives for Solar Cells*, J. Am. Chem. Soc. **130** (2008) 732-742.

[13] S. Athanasopoulos, J. Kirkpatrick, D. Martinez, J. Frost, C. M. Foden, A. B. Walker, and J. Nelson, *Predictive Study of Charge Transport in Disordered Semiconducting Polymers*, Nano. Lett. **7** (2007) 1785–1788.

[14] Yaping Li and Jolanta B. Lagowski, *Charge Carrier Mobility in Conjugated Organic Polymers - Case Studies Using Multi-Step Computational Approach*, Polymer **52** (2011) 4841–4850.

[15] Matthias Ballauff, *Stiff-Chain Polymers - Structure, Phase Behavior, and Properties*, Angew. Chem. Int. Ed. **28** (1989) 253–267.

[16] Gui-Zhong Yang, Wei-Zhi Wang, Min Wang, and Tianxi Liu *Side-Chain Effect on the Structural Evolution and Properties of Poly(9,9-dihexylfluorene-alt-2,5-dialkoxybenzene Copolymers*, J. Phys. Chem. B **111** (2007) 7747–7755.

[17] Seiji Tsuzuki, *Interactions with Aromatic Rings*, Struct. Bond. **115** (2005) 149–193.

[18] S. R. Amrutha and M. Jayakannan, *Probing the pi-Stacking Induced Molecular Aggregation in pi-Conjugated Polymers, Oligomers, and their Blends of p-Phenylenevinylenes*, J. Phys. Chem. B. **112** (2008) 1119–1129.

[19] Ludwik Leibler, *Theory of Microphase Separation in Block Copolymers*, Macromolecules **13** (1980) 1602–1617.

[20] Yanhou Geng, Sean W. Culligan, Anita Trajkovska, Jason U. Wallace, and Shaw H. Chen, *Monodisperse Oligofluorenes Forming Glassy-Nematic Films for Polarized Blue Emission*, Chem. Mater. **15** (2003) 542–549.

[21] Genvieve Sauve, Anna E. Javier, Rui Zhang, Junying Liu, Stefanie A. Sydlik, Tomasz Kowalewski, and Richard D. McCullough, *Well-Defined, High Molecular Weight Poly(3-alkylthiophene)s in Thin-Film Transistors: Side Chain Invariance in Field Effect Mobility*, J. Mater. Chem. **20** (2010) 3195–3201.

[22] Bettina Friedel, Christopher R. McNeil, Neil C. Greenham, *Influence of Alkyl Side-Chain Length on the Performance of Poly(3-alkylthiophene)/Polyfluorene All-Polymer Solar Cells*, Chem. Mater. **22** (2010) 3389–3398.

[23] Matti Knaapila, and Michael J. Winokur, *Structure and Morphology of Polyfluorenes in Solutions and Solid State*, Adv. Polym. Sci. **212** (2008) 227–272.

[24] Robert Abbel, Albertus P. H. J. Schenning, and E. W. Meijer *Fluorene-Based Materials and their Supermolecular Properties*, J. Pol. Sci.: Part A: Pol. Chem. **47** (2009) 4215–4233.

[25] Jessica M. Winfield, Antoine Van Vooren, Moo-Jin Park, Do-Hoon Hwang, Jerome Cornil, Je-Seon Kim, and Richard H. Friend, *Charge-Transfer Character of excitons in Poly[2,7-(9,9-di-n-octylfluorene)$_{(1-x)}$-co-4,7-(2,1,3-benzothiodiazole)$_{(x)}$]*, J. Chem. Phys. **131** (2009) 035104-1-035104-5.

[26] Carrie L. Donley, Jana Zaumseil, Jens W. Andreasen, Martin M. Nielsen, Henning Sirringhaus, Richard H. Friend, and Ji-Seon Kim, *Effects of Packing Structure on the Optoelectronic and Charge Transport Properties in Poly(9,9-di-n-octylfluorene*-alt-*benzothiadiazole)*, J. Am. Chem. Soc. **127** (2005) 12890–12899.

[27] Yaping Li and Jolanta B. Lagowski, *A Multi-Step Simulation of Electron Mobility in Fluorene-Benzothiadiazole Conjugated Polymer - Case Study*, Comp. Theo. Chem. **977** (2011) 157–162.

[28] Yaping Li and Jolanta B. Lagowski, *Charge Carrier Mobility in Conjugated Organic Polymers - Simulation of an Electron Mobility in a Carbazole-Benthiadiazole Based Polymers*, Photonics North 2011, ed. R. Kashyap, M. Tetu, and R. N. Kleiman, Proc. of SPIE **8007** (2011) 80071Z-1–80071Z-10.

[29] Christopher R. McNeill, Sebastian Westenhoff, Chris Groves, Richard H. Friend, Neil C. Greenham, *Influence of Nanoscale Phase Separation on Charge Generation Dynamics and Photovoltaic Performance of Conjugated Polymer Blends: Balancing Charge Generation and Separation*, J. Phys. Chem. C **111** (2007) 19153-19160.

[30] Ji-Seon Kim, Peter K. H. Ho, Craig E. Murphy, and Richard H. Friend, *Phase Separation in Polyfluorene-Based Conjugated Polymer Blends: Lateral and Vertical Analysis of Blend Spin-Cast Thin Films*, Macromolecules **37** (2004) 2861 2871.

[31] G. G. Malliaras and J. C. Scott, *The Role of Injection and Mobility in Organic Light Emitting Diodes*, J. Appl. Phys. **83** (1998) 5399–5403.

[32] P. W. M. Blom, M. J. M. de Jong, and S. Breedijk, *Temperature Dependent Electron-Hole Recombination in Polymer Light-Emitting Diodes*, Appl. Phys. Lett. **71** (1997) 930–932.

[33] Heinz Bassler, *Injection, Transport and Recombination of Charge Carriers in Organic Light-Emitting Diodes*, Polym. Adv. Technol. **9** (1998) 402–418.

[34] Benjamin J. Schwartz, *Conjugated Polymers as Molecular Materials: How Chain Conformation and Film Morphology Influence Energy Transfer and Interchain Interactions*, Annu. Rev. Phys. Chem. **54** (2003) 141-172.

[35] E. Lewars, *Computational Chemistry: Introduction to the Theory and Applications of Molecular and Quantum Mechanics*, London,(2003).

[36] W. J. Hehre, L. Radom, P. V. R. Schleyer and J. A. Pople, *Ab Initio Molecular Orbital Theory*, New York, Ch. 2 (1986).

[37] M. J. S. Dewar, *Molecular Orbital Theory of Organic Chemistry*, McGraw-Hill, New York (1969).

[38] a) J. C. Slater, *Phys. Rev. B.*, **35** 210 (1960). b) V. Fock and Z. Physik, *Phys. Rev. A.*, **61** (1930) 126

[39] J. A. Pople and D. L. Beveridge, *Approximation Molecular Orbital Theory*, McGraw-Hill, New York, Ch. 1 and 2 (1970).

[40] I. N. Levine, *Quantum Chemistry*, Prentice Hall, Engelwood Cliffs, New Jersey (2000).

[41] D. R. Hartree, *Proc. Camb. Phil Soc.*, **24** (1928) 189.

[42] A. Szabo and N. S. Ostlund, *Modern Quantum Chemistry. Macmillan*, New York (1982).

[43] R. F. W. Bader, *Atoms in Molecules*, Oxford University Press, New York (1982).

[44] R. G. Parr and W. Yang, *Density-Functional Theory of Atoms and Molecules*, Oxford University Press, New York (1989).

[45] a) E. Wilson, *Chem. Eng. News.*, **12** (1988) 330. b) D. Malakoff, *Science*, **282** (1998) 610

[46] a) I. N. Levine, *Quantum Chemistry, Prentice Hall*, New Jersey, Saddle River (2000). b) P. Hohenberg and W. Kohn, *Phys. Rev. A.*, **140** (1965) 1133

[47] W. Kohn and L. J. Sham, *Phys. Rev. A.*, **140** (1965) 1133

[48] F. Jensen, *Introduction to Computational Chemistry*, New York **101** (1997) 208

[49] a) A. Whitaker, *Einstein, Born and the Quantum Dilemma, Cambridge University Press, Cambridge*, (1996). b) V. J. Stenger, *The Unconsious Quantum*, Prometheus, Amherst, New York, (1995)

[50] J. W. Mintmire and C. T. White, *Phys. Rev. B.*, **35** (1987) 8

[51] S. H. Vosko, L. Wilk and M. Nusair, *Can. J. Phys.*, **58** (1980) 1200

[52] R. M. Dreizler and E. K. U. Gross, *Density Functional Theory*, Springer Verlag, Berlin (1990)

[53] P. J. Stephens, F. J. Devlin, C. F. Chablowski and M. J. Frisch, *J. Phys. Chem.*, **98** (1994) 11623

[54] Gaussian 09, Revision A.02, M. J. Frisch, G. W. Trucks, H. B. Schlegel, G. E. Scuseria, M. A. Robb, J. R. Cheeseman, G. Scalmani, V. Barone, B. Mennucci, G. A. Petersson, H. Nakatsuji, M. Caricato, X. Li, H. P. Hratchian, A. F. Izmaylov, J. Bloino, G. Zheng, J. L. Sonnenberg, M. Hada, M. Ehara, K. Toyota, R. Fukuda, J. Hasegawa, M. Ishida, T. Nakajima, Y. Honda, O. Kitao, H. Nakai, T. Vreven, J. A. Montgomery, Jr., J. E. Peralta, F. Ogliaro, M. Bearpark, J. J. Heyd, E. Brothers, K. N. Kudin, V. N. Staroverov, R. Kobayashi, J. Normand, K. Raghavachari, A. Rendell, J. C. Burant, S. S. Iyengar, J. Tomasi, M. Cossi, N. Rega, J. M. Millam, M. Klene, J. E. Knox, J. B. Cross, V. Bakken, C. Adamo, J. Jaramillo, R. Gomperts, R. E. Stratmann, O. Yazyev, A. J. Austin, R. Cammi, C. Pomelli, J. W. Ochterski, R. L. Martin, K. Morokuma, V. G. Zakrzewski, G. A. Voth, P. Salvador, J. J. Dannenberg, S. Dapprich, A. D. Daniels. Farkas, J. B. Foresman, J. V. Ortiz, J. Cioslowski, and D. J. Fox, Gaussian, Inc., Wallingford CT, (2009).

[55] A. D. Becke, Density-Functional Thermochemistry. III. The Role of Exact Exchange, J. Chem. Phys., **98** (1993) 5648–52.

[56] A. D. Becke, *Density-Functional Exchange-Energy Approximation with Correct Asymptotic-Behavior*, Phys. Rev. A **38** (1988) 3098–3100.

[57] S. H. Vosko, L. Wilk, and M. Nusair, *Accurate Spin-Dependent Electron Liquid Correlation Energies for local Spin Density Calculations: A Critical Analysis* , Can. J. Phys. **58** (1980) 1200–1211.

[58] C. Lee, W. Yang, and R. G. Parr, *Development of the Colle-Salvetti Correlation-Energy Formula into a Functional of the Electron Density*, Phys. Rev. B. **37** (1988) 785–789.

[59] Axel D. Becke, *Density-Functional Thermochemistry. V. Systematic Optimization of Exchange-Correlation Functionals*, J. Chem. Phys. **107** (1997) 8554–8560.

[60] Stefan Grimme, *Semiempirical GGA-type Density Functional Constructed with a Long-Range Dispersion Correction*, J. Comp. Chem. **27** (2006) 1787–1799.

[61] Stefan Grimme, Jens Antony, Stephan Ehrlich, and Helge Krieg, *A Consistent and Accurate Ab Initio Parametrization of Density Functional Dispersion Correction (DFT-D) for the 94 Elements H-Pu*, J. Chem. Phys. **132** (2010) 154104–154122.

[62] Stefan Grimme, Stephan Ehrlich, Lars Goerigk, *Effect of the Damping Function in Dispersion Corrected Density Functional Theory*, J. Comp. Chem. **32** (2011) 1456–1465.

[63] C. Pisani (Ed.) *Lecture Notes in Chemistry: Quantum-Mechanical Ab-Initio Calculation of the Properties of Crystalline Materials*, Spring-Verlang, Heidelberg, **67** (1996).

[64] N. W. Ashcroft and N. D. Mermin, *Solid State Physics*, Cornell University (1976)

[65] E. Runge, E. K. U. Gross, *Density-Functional Theory for Time-Dependent Systems*, Phys. Rev. Lett. **52** (1984) 997–1000.

[66] A. J. W. Tol, Synth. Met. **74** (1995) 95.

[67] A. J. W. Tol, Chem. Phys. **208** (1996) 73.

[68] G. Brocks, Synth. Met. **102** (1999) 914.

[69] M.E. Casida, C. Jamorski, F. Bohr, J. Guan, and D.R. Salahub, Ed. by S. P. Karna and A. T. Yeates *Theoretical and Computational Modeling of NLO and Electronic Materials*, ACS Press. Washington, D.C. (1996)

[70] Stefan Grimme, *Accurate Description of van der Waals Complexes by Density Functional Theory Including Empirical Corrections*, J. Comp. Chem. **25** (2004) 1463–1473.

[71] Stefan Grimme, *Density Functional Theory with London Dispersion Corrections*, WIREs Comp. Mol. Sci. **1** (2011) 211–228.

[72] Lin Ling and Jolanta B. Lagowski, *Electronic band structure of alternating fluorene-oxadiazole conjugated copolymer - A 1D solid-state DFT study*, J. Mol. Struct.: Theochem **994** (2010) 146-155.

[73] Klaus Muller-Dethlefs and Pavel Hobza, *Noncovalent Interactions: A Challenge for Experiment and Theory*, Chem. Rev. **100** (2000) 143–168.

[74] Konstantin N. Kudin and Gustavo E. Scuseria, *A Fast Multipole Method for Period Systems with Arbitrary Unit Cell Geometries*, Chem. Phys. Lett. **283** (1998) 61-68.

[75] Konstantin N. Kudin and Gustavo E. Scuseria, *A Fast Multipole Algorithm for the Efficient Treatment of the Coulomb Problem in Electronic Structure Calculations of Period Systems with Gaussian Orbitals*, Chem. Phys. Lett. **289** (1998) 611 616.

[76] Konstantin N. Kudin and Gustavo E. Scuseria, *Linear-Scale Density-Functional Theory with Gaussian Orbitals and Period Boundary Conditions: Efficient Evaluation of Energy and Forces via the Fast Multipole Method*, Phys. Rev. B. **61** (2000) 16440–16453.

[77] Oleg V. Yazyev, Konstantin N. Kudin, and Gustavo E. Scuseria, *Efficient Algorithm for Band Connectivity Resolution*, Phys. Rev. B. **65** (2002) 205117-1 205117-8.

[78] R. Bauernschmitt and R. Ahlrichs, *Treatment of Electronic Excitations within the Adiabatic Approximation of Time Dependent Density Functional Theory*, Chem. Phys. Lett. **256** (1996) 454–464.

[79] M. E. Casida, C. Jamorski, K. C. Casida, and D. R. Salahub, *Molecular Excitation Energies to High-Lying Bound States from Time-Dependent Density-Functional Response Theory: Characterization and Correction of the Time-Dependent Local Density Approximation Ionization Threshold*, J. Chem. Phys. **108** (1998) 4439–4449.

[80] R. E. Stratmann, G. E. Scuseria, and M. J. Frisch, *An Efficient Implementation of Time-Dependent Density- Functional Theory for the Calculation of Excitation Energies of Large Molecules*, J. Chem. Phys. **109** (1998) 8218–24.

[81] C. Van Caillie and R. D. Amos, *Geometric Derivatives of Density Functional Theory Excitation Energies Using Gradient-Corrected Functionals*, Chem. Phys. Lett. **317** (2000) 159–164.

[82] F. Furche and R. Ahlrichs, *Adiabatic Time-Dependent Density Functional Methods for Excited State Properties*, J. Chem. Phys. **117** (2002) 7433–7447.

[83] S. I. Gorelsky, SWizard program, http://www.sg-chem.net/, University of Ottawa, Ottawa, Canada (2010): S. I. Gorelsky and A. B. P. Lever, *Electronic Structure and Spectra of Ruthenium Diimine Complexes by Density Functional Theory and INDO/S. Comparison of the Two Methods*, J. Organomet. Chem. **635** (2001) 187-196.

[84] GaussView (Version 4.1.2) Visualization Software, Semichem Inc., Shawnee Mission KS, (2000-2006).

[85] Zhijun Gong and Jolanta B. Lagowski, *Density Functional Study of the Electronic and Optical Properties of Fluorene-thieno[3,2-b]thiophene-Based Conjugated Copolymers*, Mol. Sim. **35** (2009) 737-747.

[86] Stefan Gamerith, Christoph Gadermaier, Ullrich Scherf, and Emil J.W. List, *Emission Properties of Pristine and Oxidatively Degraded Polyfluorene Type Polymers*, phys. stat. sol. **201** (2004) 1132–1151.

[87] J. Ding, Y. Tao, M. Day, J. Roovers and M. D'Iorio *Electrochemical and Fluorescent Properties of Alternating Copolymers of 9,9-dictofluorene and Oxadiazole as Blue Electroluminescent and Electron Transport Materials*, J. Opt. A: Pure Appl. Opt. **4** (2002) S267–S272.

[88] R. E. Gerkin, A. P. Lundstedt and W. J. Reppart *Structure of Fluorene, C13H10 at 159 K*, Acta Crystallographica **40** (1984) 1892–1894.

[89] Michael J. Banach, Richard. H. Friend, and Henning Sirringhaus, *Influence of the Casting Solvent on the Thermotropic Alignment of Thin Liquid Crystalline Polyfluorene Copolymer Films*, Macromolecules **37** (2004) 6079–6085.

[90] Valentina Marcon, Nico van der Vegt, Gerhard Wegner, Guido Roas, *Modeling of Molecular Packing and Conformation in Oligofluorenes*, J. Phys. Chem. B **110** (2006) 5253–5261.

[91] S. Kawana, M Durrell, J. Lu, J. E. Macdonald, M. Grell, D. D. C. Bradley, P. C. Jukes, R. A. L. Jones, S. L. Bennett, *X-ray Diffraction Study of the Structure of Thin Polyfluorene Films*, Polymer **43** (2002) 1907–1913.